2024 SADIA YOUNIS SU92-MSCHW-F22-020 FOS

Controlling Porosity In Iron-Doped Silica Nanoparticles For Drug Delivery In Cancer Treatment

SUPERIOR UNIVERSITY

Thesis Submitted to

The Superior University Lahore

In Partial Fulfillment of the

Requirement for the Degree of

M.Phil Chemistry

By

SADIA YOUNIS

Roll No. SU92-MSCHW-F22-020

Session: 2022-2024

Faculty of Sciences

Controlling Porosity In Iron-Doped Silica Nanoparticles For Drug Delivery In Cancer Treatment

SUPERIOR UNIVERSITY

Thesis Submitted to

The Superior University Lahore

In Partial Fulfillment of the

Requirement for the Degree of

M.Phil Chemistry

By

SADIA YOUNIS

Roll No. SU92-MSCHW-F22-020

Session: 2022-2024

Faculty of Sciences

Author's Declaration

I hereby state that my M.Phil thesis titled **"Controlling porosity in iron-doped silica nanoparticles for drug delivery in cancer treatment"** is my work and has not been submitted previously by me for taking any degree from this University,

The Superior University, Lahore

or anywhere else in the country/world.

At any time if my statement is found to be incorrect even after my graduation, the university has the right to withdraw my M.Phil degree.

Name of Student: Sadia Younis

Date: _____

Plagiarism Undertaking

I solemnly declare that research work presented in the thesis titled **"Controlling Porosity In Iron-Doped Silica Nanoparticles For Drug Delivery In Cancer Treatment"** is solely my research work with no significant contribution from any other person. Small contribution/help wherever taken has been duly acknowledged and that complete thesis has been written by me.

I understand the zero-tolerance policy of the HEC and University,

The Superior University, Lahore

towards plagiarism. Therefore, I as author of the above-titled thesis declare that no portion of my thesis has been plagiarized and any material used as a reference is properly referred/cited. I undertake that if I am found guilty of any formal plagiarism in the above-titled thesis, even after awarding of M.Phil. degree, the University reserves the rights to withdraw/revoke my M.Phil. degree and that HEC and the University have the right to publish my name on the HEC/University website on which names of students are placed who submitted a plagiarized thesis.

Student/Author Signature: _____

Name: Sadia Younis

Research Completion Certificate

This is to certify that the thesis entitled **"Controlling porosity in iron-doped silica nanoparticles for drug delivery in cancer treatment"** submitted by **"Sadia Younis"** has been accepted towards the partial fulfillment of the requirement for M.Phil. **"Chemistry"**. The quality of the work contained in this thesis is adequate for the award of degree.

Supervisor Name: Dr. Quratulain Amjad

Designation: Assistant Professor

Signature: _____

Certificate of Approval

This is to certify that the research work presented in this thesis, titled **"Controlling porosity in iron-doped silica nanoparticles for drug delivery in cancer treatment"** was conducted by **"Sadia Younis"** under the supervision of **"Dr. Quratulain Amjad"**

No part of this thesis has been submitted anywhere else for any other degree. This thesis is submitted to the Faculty of Sciences, The Superior University, Lahore in partial fulfillment of the requirements for the degree of Master of Philosophy in the field of **"Chemistry"** in Faculty of Sciences at The Superior University, Lahore.

Student Name: Sadia Younis Signature:_____

Examination Committee:

Session Chair: Signature:_____

a) External Examiner: Signature:_____

b) Internal Examiner: Signature:_____

c) Supervisor Name: Dr. Quratulain Amjad Signature:_____

d) Name of HOD: Prof. Dr. Uqba Mehmood Signature:_____

e) Name of Dean: Prof. Dr. Mohammad Naveed Babur Signature:_____

f) Controller Examination: Dr. Muhammad Haris Signature:_____

Dedication

To my respected family and supervisor,

They motivated me to embark on all of my adventures,

especially this one, and without them, I would be nothing.

Thank them for having confidence in me.

You are my primary source of inspiration and motivation.

Acknowledgments

In the name of Allah, the kindest and most sympathetic. All admire Almighty Allah, Who helps and guides us in every darkness of life. Special thanks to Allah Almighty, who showed me courage, patience, and good health, all because I can complete my thesis. All respect and dignity for our Holy Prophet Muhammad (PBUH), Who showed us a light of the right path and provided guidance for us in all aspects of life.

I am highly grateful to my honorable and polite supervisor, Dr. Quratulain Amjad, and my co-supervisor, Dr. Fizza Naseem for her continuous motivation and encouragement, inspiring guidance, notable suggestions, active supervision, informed advice, and valuable discussions that led me towards the noteworthy design of thesis.

I want to express my sincere gratitude to Prof. Dr. Muhammad Naveed Babur, the Dean of Superior University, Prof. Dr. Uqba, the Head of Department, and all the other teachers who have helped me along the way. My growth as a researcher has been greatly aided by your influence, particularly in the beginning of my studies.

I wish to acknowledge with indebted thanks the valuable help of my class fellows, friends, and all the lab attendants from Superior University for their kind guidance and support. I would especially like to thank my classmate Abu Sufyan for his constant emotional support during this study. I was able to endure difficult circumstances because of his support and faith in me. Finally, I would want to express my gratitude to my parents for their tolerance, steadfast support, and constant inspiration. This achievement is the result of their love and devotion.

Ultimately, I am humbly thankful to Almighty Allah, who gave me the courage and abilities to complete this study.

Sadia Younis

Table of Contents

Page

List of Tables

Description **Page**

List of Figures

Description **Page**

List of Abbreviations

HCC	Hepatocellular Carcinoma
FeMS(C)	Iron Doped Silica Nanoparticles With CTAB Surfactant
FeMS(S)	Iron Doped Silica Nanoparticles With SDS Surfactant
FeMS(DA)	Iron Doped Silica Nanoparticles With Diammonium Quarternary Salt
XRD	X-Ray Diffraction
UV-Vis	Ultraviolet-Visible Spectroscopy
SEM	Scanning Electron Microscopy
FT-IR	Fourier-Transform Infrared Spectroscopy
BET	Brunauer–Emmett–Teller
TGA	Thermogravimetric analysis
Fe_3O_4	Magnetite
ROS	Reactive Oxygen Species
CCA	Cholangiocarcinoma
HBsAg	Hepatitis B Surface Antigen
HBV	Hepatitis B Virus
HCV	Hepatitis C Virus
NPs	Nanoparticles
IARC's	International Agency For Research On Cancer
SPIONS	Superparamagnetic Iron Oxide Nanoparticles
Fe_3O_4	Magnetite
ROS	Reactive Oxygen Species
MSN	Mesoporous Silica Nanoparticles
MCM	Mobile Crystalline Of Materials
SBA-X	Santa Barbara Amorphous
IUPAC	International Union Of Pure And Applied Chemistry
γ-Fe_2O_3	Maghemit
IONP	Iron Oxide Nanoparticles
TEOS	Tetraethyl Orthosilicate
CMC	Critical Micelle Concentration
CTAC	Cetyltrimethylammonium Chloride
C18TMS	Noctadecyltrimethoxysilane
CTAB	Cetyltrimethylammonium Bromide
EPR	Enhanced Permeation And Retention
DDS	Drug-Delivery Systems
TEM	Transmission Electron Microscopy
EMT	Epithelial Mesenchymal Transition
NF-kB	Nuclear Factor Kappa-B
PI3K/AKT	Phosphatidylinositol 3 Kinase/Protein Kinase B
MAPK/ERK	Mitogen-Activated Protein Kinase/Extracellular Regulated Protein Kinases
COVID-19	Coronavirus Disease 2019
SVR	Sustained Virological Response
NASH	Non-Alcoholic Steatohepatitis
NSM	Nanostructured Materials
SiO_2	Silicon Dioxide
SiNPs	Silica Nanoparticles
MSMs	Mesoporous Silica Materials
$FeCl_2 \cdot 4H_2O$	Iron (II) Chloride Tetrahydrate
$FeCl_3.6H_2O$	Iron (III) Chloride Hexahydrate
SDS	Sodium Dodecyl Sulfate
DA	Diquaternary Ammonium Salt

HCl	Hydrochloric Acid
NaOH	Sodium Hydroxide
SO	Sorafenib Tosylate
MTT	3- (4, 5 dimethylthiazolyl-2)-2, 5-diphenyltetrazolium bromide
PBS	Phosphate Buffered Saline
DMEM	Dulbecco's Modified Eagle's Medium
FBS	Fetal Bovine Serum

ABSTRACT

Hepatocellular carcinoma (HCC) is still a difficult clinical problem in oncology sorafenib is one of the best chemotherapeutic agents. But unfortunately, its clinical utilization is hampered due to poor aqueous solubility, high dosage requirements, off-target toxicity, and the emergence of drug resistance. In order to address these shortcomings, we designed and optimized iron-doped silica (FeMS(C), FeMS(S), and FeMS(DA)) nanoparticles with controlled porosity to enhance drug delivery efficiency and induce ferroptosis, a novel iron-dependent form of cell death for overcoming resistance in liver cancer therapy. Three types of FeMS(C), FeMS(S), and FeMS(DA) nanoparticles were fabricated using different surfactants to control porosity and structural properties. The synthesized nanocarriers were thoroughly characterized using FT-IR, UV-Vis, SEM, and XRD. Brunauer–Emmett–Teller (BET) research verified a well-defined mesoporous structure, optimum pore volume, and a very high surface area, allowing for controlled release kinetics and increased loading capacity. Porosity control was attained by utilizing mathematically precise etching method to achieve enhanced encapsulation and sustained release of sorafenib. In vitro cytotoxicity studies of HepG2 liver cancer cells exhibited recommended endocytosis capacities which lead to improved therapeutic efficacy compared to free sorafenib. Because ferroptosis is based on raising intracellular iron levels, promoting the generation of ROS, and producing lipid peroxidation, the incorporation of Fe_3O_4 in the silica matrix was beneficial. Increase in markers associated with the epithelial to mesenchymal transition further supported the possibility of decreased cell death and metastatic potential. The drug release studies also revealed a sustained and pH-triggered drug release profile that could reduce systemic toxicity while having a lasting effect. The engineered FeMS(C), FeMS(S), and FeMS(DA) nanoparticles effectively addressed the main issues of conventional sorafenib therapies, including solubility, total amount needed, and resistance to treatment via ferroptosis induction. This study demonstrated the importance of porosity engineering in the context of nanomedicine, presenting a multifunctional platform for targeted efficacious treatment for liver cancer and adds considerable insight into further translational research into ferroptosis therapeutics and enhanced drug delivery systems.

CHAPTER 1

INTRODUCTION

1.1 Cancer

Worldwide, a large percentage of deaths are caused by cancer [1]. Previously the third leading cause of death in 1990, cancer accounted for over 8 million deaths globally in 2013, so it is the second most prevalent reason of death after heart disease [2]. Since the number of cancer survivors is still rising [3], the main players in the healthcare industry—patients, providers, and payers—should determine which cancer patients are most likely to die and from what cause [4]. Cancer results from transformation of a normal cell into a tumor cell resulting in indefinite proliferation. In this multi stage process the cells, very often, acquire the ability migrate and colonize neighboring or distant tissue, thus becoming metastatic [5]. The deaths caused by cancer are primarily due to organ failure and metastasis, or the spread of primary tumor cells to other sites [6].

1.1.1 Introduction To Cancer Metabolism

The metabolic status of normal differentiated cells and cancer cells are distinct from each other. In order to produce the energy needed for cellular function and equilibrium, normal cells absorb nutrients like glucose and rely on oxidative phosphorylation in the mitochondria [7]. Further, normal cells are supported by the collaboration between intracellular signaling pathways and metabolic pathways to supply energy and promote growth in a controlled manner [8, 9]. In contrast, cancer cells exhibit deregulation of oncogenic pathways that reprogram metabolism to induce uncontrolled proliferation and tumor growth [8, 9].

1.2 Liver Cancer

Liver cancer is an aggressive disease that is becoming more common worldwide [10]. Liver cancer is most frequent, severe malignancies and the second leading cause of cancer-related death globally [1]. Liver cancer is the second leading cause of cancer mortality in men and the sixth leading cause in women worldwide [11].

1.2.1 Liver Cancer Sub-Types

Liver cancer has several subtypes, each of which has a unique mutational signature. Hepatocellular carcinoma (HCC), most significantly common kind of primary cancers of the liver accounts for around 85% of cases in the clinic [12, 13]. HCC is driven by oncogenic transcription factors that direct cellular responses that are still poorly understood at the molecular level. HCC originates from transformed hepatocytes as a result of genomic and environmental insults [12, 13]. Another sub-types of liver cancer are hepatoblastoma, and Cholangiocarcinoma (CCA).

1.2.2 Liver Cancer As Chronic Disease

Liver cancer arises in the context of chronic liver disease, which is often caused by underlying environmental and genetic factors [14]. Hepatocarcinogenesis is a complex process that occurs over an extended period of time as somatic mutations accumulate in the liver. Next generation sequencing technology has pinpointed the genetic alterations that are the main drivers of hepatocarcinogenesis. These cancer-causing mutations- can be classified into either oncogenic (gain of function) or tumor suppressor (loss of function). These genes are involved in key cellular processes, including telomere regulation, cell cycle control, chromatin modification, and oxidative stress [12].

1.2.3 Risk Factor

Genetic factors work together with environmental factors such as viral infections, environmental toxins, obesity, and alcohol to promote liver tumorigenesis [12]. While viral hepatitis infections pose a significant risk for HCC, the incidence of metabolic syndrome associated HCC cases is also increasing, especially in the West [12, 14].

1.2.3.1 Viruses That Cause Hepatitis

Chronic HBV infection has been recognized as an etiologic cause for the development of HCC for more than 40 years [15]. The regions with the greatest incidence of chronic HBV infection are home to about 45% of the world's population [16]. Chronic infection with HBV is measured using seropositivity for hepatitis B surface antigen (HBsAg). The relative risk associated with seropositivity of HBsAg and liver cancer ranges from 5.3-148 in cohort studies, and 5 to 30 in case control studies [17]. HCV has been identified as a carcinogen to humans since the early 1990s [17]. Anti-HCV

antibodies are frequently used to detect chronic HCV infection. Relative risks for chronic HCV infection have been found to range from approximately 15 to 25.

Few extensive studies focusing on the population have reported the amount of hepatitis B and C infections, making it difficult to estimate the prevalence internationally. Nonetheless, according to certain research, 5–20% of people with a persistent HBV infection also have an HCV infection [18].

The combined effects of HBV and HCV have been the subject of contradicting meta-analyses, which have found both sub-additive and super-additive effects (sub-additive [19], and super-additive [20, 21]). More recent studies (2000-2009), cohort studies, and studies carried out in regions where HBV and HCV infection were rare showed an overall sub-additive effect on risk of hepatocellular carcinoma, while HBV endemic areas showed an additive effect, and older studies, case-control studies, and HCV endemic areas showed a super-additive effect, according to Cho et al. [19].

1.2.3.2 Alcohol

Alcohol has been categorized as a group 1 carcinogen by the IARC since 1988. Cirrhosis, a significant risk factor for liver cancer, is believed to be caused by heavy drinking. Eastern and Western European nations have the greatest rates of alcohol use per capita. Heavy or "at-risk" alcohol consumption is defined by the National Institute on Alcohol Abuse and Alcoholism as more than four drinks on any one day or more than fourteen drinks per week for males, and more than three drinks on any one day or more than seven drinks per week for women [22]. According to a meta-analysis by Turati et al., heavy drinkers who consume 37.5g of ethanol (about three drinks) or more daily had a 1.16 (95% CI: 1.01-1.34) risk of liver cancer compared to those who do not, and drinking increases the risk [23].

1.2.3.3 Tobacco Smoking

Beginning in the 1950s, research has demonstrated that smoking causes cancer [24], including links between smoking and liver cancer [25]. Cigarette smoke contains more than 60 recognized carcinogens [26], including aromatic amines and polycyclic aromatic hydrocarbons, both of which have been linked to an increased risk of HCC [27]. Current smokers had almost 1.5 times the risk of liver cancer compared to never smokers, according to recent meta-analyses by Lee et al. [28] and Gandini et al. [29] (Lee et al: 1.51 [1.37,1.67]; Gandini et al: 1.56 [1.29,1.87]).

This is in line with the IARC's 2004 results in their monograph on tobacco smoke and involuntary smoking, which said that cohort and case control studies have repeatedly shown a link between tobacco use and liver cancer [25]. Alcohol consumption is common among smokers. While Lee et al. discovered that the risk ratio for current tobacco users was marginally lower after controlling for alcohol (before adjusting: 1.51, 95% CI: 1.37, 1.67; after change: 1.43, 95% CI: 1.21, 1.68), Chuang et al. discovered that the threat ratio for alcohol and liver cancer was 1.29 (95% 95% CI: 1.08, 1.50) prior to and 1.33 (95% CI: 1.15, 1.52) after controlling for smoking. [30].

1.3 Nanoparticles

Over the past 50 years, a lot of study has been done on nanoparticles (NPs), taking advantage of their tiny size, which is typically between 1 and 100 nm. Their three main characteristics are that they have a very high volume-to-surface ratio, are very mobile in the free state, and may show quantum effects that affect their electrical properties [31-33]. This could enable them to evade the body's defence mechanisms [34].

1.3.1 Types Of Nanoparticles

Nanoparticles have been categorized based on shape, size, composition, and functionality. For instance, Siegel delineated four-dimensional nanoparticle formations in 1993: These include quantum dots or nanoparticles in three dimensions, the fullerene tiny structures, a two-dimensional nanotubes made of carbon, one dimension rather graphene thin sheets, and zero-dimensional nanostructures [35]. Based on composition, we have grouped in this work nanoparticles that are pertinent to biotechnology research, such as polymeric, metallic, magnetic, inorganic, and environmentally friendly and recyclable substances make up organically nanoparticles [36]. It has been demonstrated that they have a lot of potential for drug transportation [37-40]. Polymeric, metallic, and magnetic nanoparticles are other common classifications for both nanoparticles are both inorganic and organic (Figure 1). The element used to make the frame is the primary distinction among organic and inorganic particles.

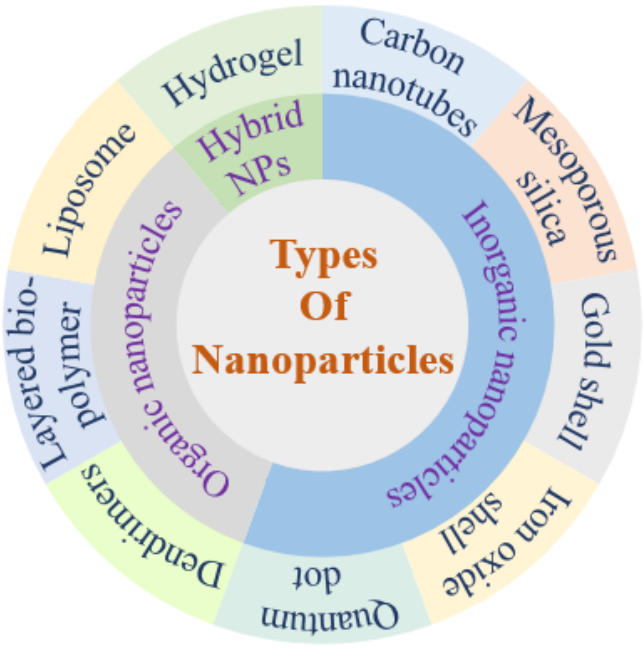

Figure 1: Illustrates the different types of nanoparticles, including inorganic, hybrid, and organic nanoparticles.

1.3.1.1 Organic Nanoparticles

As the name suggests, organic nanoparticles are ultimately biological in origin and are formed from carbon-containing substances. Among many others, dendrimers, liposomes, and micelles are examples. These kinds of nanoparticles are frequently used in food technology and medication administration [41, 42].

1.3.1.2 Inorganic Nanoparticles

Nanoparticles that are not biologically derived and do not include carbon are referred to as inorganic. These nanoparticles, which have been widely used Silicon tiny particles, tiny gold quantum dots, and nanoparticles made from superparamagnetic iron oxide (SPIONS) are a few examples of materials used in biomedical applications such as contrasting agents and for cancer treatment. [43, 44].

i) Mesoporous Silica Nanoparticles

The silica nanoparticles are a major unit in designing and engineering nanostructures for a wide range of application. These particles comprise of porous and nonporous. However, the mesoporous silica nanoparticles (MSN) are of greater interest because of highly ordered structures with larger surface areas. Mesoporous nanoparticles are classified by the IUPAC as having spherical or cylindrical forms and pores that range

in size from 2 to 50 nm [45]. In 1992, Mobile Corporation laboratories synthesized the MSN, which was initially published under the designation MCM-X (Mobile Crystalline of Materials) [46]. This became the starting point to broadly use MSN in the field of research. Even before this, there was a patent in 1971 to synthesize low-density silica using a cationic surfactant [47]. In 1998, Zhao et al. [48, 49] synthesized MSN using a non-ionic triblock surfactant. They called it SBA-X (Santa Barbara Amorphous), where X stands for the particular surfactant and pore structure that were used in the synthesis. For example, SBA-15 refers using P123 surfactant to produce hexagonally ordered cylindrical pores and SBA-16 refers using F127 surfactant to produce spherical pores centred in cubic structure. SBA-15 mesoporous particles synthesized using non-ionic surfactant Pluronic triblock copolymer P123. The surfactant forms micelles that acts as a template to form mesoporous structure while synthesizing the particles. They are highly ordered cylindrical pores in hexagonal orders with pore ranges from 2-26 nm [48-50]. MSN have variable pore length from 200 nm to several microns [51]. MSN have a huge surface area and highly depends on the procedure and applications, and a high value of 838 m^2/g of the particles was reported in literature [52].

ii) Nanoparticles Of Superparamagnetic Iron Oxide

Because of their high magnetic susceptibility, low Curie temperature, and multivalent oxidation states, iron oxide nanoparticles find extensive utility [53, 54]. The most studied particles are Magnetite (Fe_3O_4) and Maghemite (γ-Fe_2O_3) [55]. Magnetite is a black ferromagnetic mineral that contains iron in both Fe (II) and Fe (III) oxidation states. The reddish-brown ferromagnetic mineral known as maghemite is low in iron (II). Magnetite is a promising candidate for biomedical application with proven biocompatibility [56]. The iron oxide nanoparticles (IONP) exhibit quantum size effect showing superparamagnetic property. The superparamagnetism is the unique property of Fe_3O_4 in small, single-domain particles without magnetic memory. To put it succinctly, ferromagnetic particles, such as iron, appear as single-domain magnetic particles when they are reduced in size to less than 40 nm. When exposed to an external magnetic field, the particles develop strong internal magnetization due to electron exchange coupling, creating a superparamagnetic iron oxide nanoparticle [57]. The superparamagnetic iron oxide nanoparticles (SIONP) are synthesized employing physical (aerosol, powder ball milling, gas phase deposition, etc.), chemical (co-

precipitation, microemulsion, hydrothermal, chemical, thermal decomposition, etc.), and biological (fungi, bacteria, and protein-mediated) approaches [58]. Applications for SPION in biomedicine include medication delivery, bioseparations, and in vitro cell manipulation [59-61]. The United State and European Union regulation agencies had approved to incorporate SPION in commercial MRI formulation due to the better in vivo contrast [62]. These nano size SIONP can be transported in the desired direction by applying magnetic field but does not exhibit magnetic memory allowing them to disperse in the suspension.

iii) Applications of Silica Coating On Magnetite Nanoparticles

Because of its improved chemical stability, biocompatibility, and capacity to inhibit magnetite core oxidation and agglomeration throughout a wide pH range, among the most useful and promising coating components is silica [63]. Silica-coated core-shell nanoparticles have been discovered to disperse well in aqueous solutions due to the hydrophilic nature of silica [58]. Additionally, silica's surface is frequently completed with a silanol group, which can conjugate with a range of biomolecules and particular ligands by reacting with different chemicals and silane coupling agents [64]. Currently the Stöber method [65, 66] and microemulsion method [67-69], are two of the most popular ways to make silica-covered nanoparticles of haematite. The first is applied to magnetite nanoparticles that dissolve in water, while the second is a great substitute approach to non-polar in nature solvent-dispersed magnetite with silica covering [58]. In 1994, Philipse et al. reported using a sol-gel technique to coat magnetite nanoparticles with silica for the first time [70].

1.4 Synthesis Method Of Nanoparticles

1.4.1 The Stober Method

By hydrolyzing and polycondensing silica sources like tetraethyl orthosilicate (TEOS) in ethanol solution with water and ammonia acting as a catalyst, the Stöber process creates silica shells [65, 71, 72]. Large aggregates and the generation of polydisperse products are unavoidable in this approach due to the high hydrolysation rate of TEOS [64]. Numerous researchers have looked into ways to improve the coating qualities of the nanoparticles using variations of the Stöber approach [73]. A systematic investigation of the sol-gel approach for the creation of silica-coated core-shell magnetic nanoparticles has been described by Deng et al. Their results demonstrated

that the kind of alcohol, the alcohol to water volume proportion, the catalyst's quantity , and its precursor quantity were three important reaction parameters that affected the synthesis of nanoparticles. Additionally, they noticed that the magnetite nanoparticles covered with silica exhibited superparamagnetic properties [72]. An enhanced method for coating magnetite nanoparticles to produce a stable core-shell colloid has been presented by Sun et al. Citric acid was initially added to magnetite nanoparticles made using the co-precipitation process as part of their procedure. A pretreatment with a diluted silicate solution and a subsequent Stöber procedure in ethanol were used to regulate the silica coating [74]. The impact of the volume ratio between the magnetite colloidal and tetraethyl orthosilicate (TEOS) on the combination of nanoparticles' morphological ones such, structural, and magnetic properties has been thoroughly examined by Gao et al. Additionally, they demonstrated that the thermal stability of magnetite nanoparticles was enhanced by their silica covering [75]. According to Kulkarni et al., coprecipitation in a modified Stöber process produces magnetite nanoparticles with exceptional stability and a silica covering that inhibits magnetic particle aggregation [76]. According to Sonmez et al., particles of silica with diameters ranging from 5 to 200 nm can be produced by altering (TEOS) proportion to H_2 O and NH_3 concentrations [64].

1.4.2 The Microemulsion Method

The nanoparticles might be coated with consistent silica layers using the microemulsion technique. Water, oil, and amphiphilic surfactant are the three primary ingredients in this process. This technique surrounds the nano-droplet-shaping nano-reactors with reverse micelles or surfactant-based micelles to regulate applying a silica layer to magnetic nanoparticles. The highly monodisperse yield is a benefit of the reverse micelle's constrained nano-reactor environment. Since the size of the nanoparticles is directly correlated with the molar ratio between H_2O and surfactant, which controls the size of the nano-droplets, the silicate layer's size can be adjusted. The micro-emulsion in reverse technique may create homogeneous silica shells as thin as 1 nm [77]. This method's benefit is so the dimensions of the particles might be easily regulated by varying the reactant content, ageing duration, and the molar ratio of water to surfactant. Nevertheless, the yield of reverse microemulsion synthesis is said to be low [53, 64]. Additionally, the use of harmful organic solvents and surfactants necessitates thorough washing prior to any biological applications in order to prevent

the surfactant molecules from disrupting or lysing biomembranes, making the process long, costly, and less environmentally friendly [53, 64]. Santra et al. created silica-coated iron oxide nanoparticles using the water-in-oil microemulsion technique. They investigated how the size, magnetic characteristics, and crystallinity of the particles were affected by the three surfactants that are non-ionic are Brij-97, Igepal CO520, and Triton X-100. They have produced homogeneous core-shell silica-magnetite nanoparticles with a 1 nm shell thickness. They have demonstrated how the surfactants's molecular composition affects how surfactant molecules adsorb onto the outer layer of nanoparticles. Additionally, they demonstrated that a stronger particle aggregation of the more hydrophobic surfactant (Brij 97) might be caused by a significant -hydrophobic interaction among the neighboring nanoparticles' oleyl compounds [78]. The production of uniform dual-functional silicon-magnetite core-shell nanoparticles using (FITC)-incorporated silica has been documented by Lu et al. shells of 20 nm thickness using the microemulsion process in order to successfully label human mesenchymal stem cells [69]. Ding et al. have described methods for using a different tiny emulsion to cover particles of magnetite with silica process in order to create single-core magnetic core-shell nanoparticle, variable shell thickness, and no core-free silica nanoparticle production. According to their findings, the ferromagnetic size should be taken into consideration when selecting the silicone coating specifications. As a result, parameters that work well for magnetite nanoparticles of a particular size may not work well for particles of a different size range. They also mentioned how crucial it is to modify the quantity of magnetite nanoparticles in an aqueous domain. It has been shown that a tiny aqueous domain can be used to construct extremely thick silica shells, as opposed to a bigger aquatic area is required to create thick layers. They proposed that the generation of layer free silica nanoparticles might be prevented by increasing the concentration of TEOS through the continually fractionated drops, thereby forming a thick silica shell [68].

1.5 Surfactants For Structuring

Model the surfactant templating method is used to create mesoporous silica shells by adding a surfactant at a concentration higher than the critical micelle concentration (CMC). The silica precursor would condense around the template to create a silica matrix, and the surfactant would self-aggregate to produce micelles. Thermal calcination or solvent extraction could be used to eliminate surfactant templates,

producing a mesoporous structure. The surfactant templates dictate the structure, including pore size and direction [79, 80]. Several kinds of surfactants have been used to create a wide variety of mesoporous structures with distinct pore architecture and organization [81]. Wu et al. created the first mesoporous magnetic silica nanocomposite in 2004. They created a mesoporous structure on micrometer-sized magnetite (Fe_3O_4) particles using cetyltrimethylammonium chloride (CTAC) as a template [82]. Zhao et al. created uniform spheres of mesoporous magnetic nanocomposites with a silica shell and a large surface area. Tetraethoxysilane (TEOS) and noctadecyltrimethoxysilane (C18TMS) were sol-gel polymerized simultaneously, and the organic group was then removed to create the mesoporous silica layer on top of the thin, dense silica layer that had been produced on the magnetic particle's surface [83]. Deng et al. have synthesized superparamagnetic high-magnetization microspheres having an outside layer of ordered mesoporous silica with cylindrical holes, an inner nonporous silica layer in the centre, and a magnetite core. They have created a mesoporous shell using cetyltrimethylammonium bromide (CTAB) as a template [84]. A method for optimising the formation of a porous silica coating on magnetic nanoparticles for application in drug delivery has been published by El-toni et al. The Fe3O4 nanoparticles were coated with a thick silica layer and a co-structure guided mesoporous silica layer. According to their proposal, a co-structure guiding agent can help the negatively charged surfactant molecules and negatively charged silica layers interact electrostatically [85]. According to Xue et al., they used cetyltrimethylammonium bromide (CTAB) as a pore shaping agent to create luminous mesoporous silica-coated iron oxide nanoparticles for fluorescent trimodal imaging, computed tomography, and magnetic resonance imaging. Using experimental CTAB framework as a direction, they deposited luminous dye-doped silica on top of superparamagnetic ferrous oxide nanoparticles to produce mesoporous silica-coated nanoparticles. Synthetic nanoparticles with uniform sizes showed a 20 nm mesoporous silica shell. According to reports, the surface area was 692.06 m^2/g and the average pore size was 2.7 nm [86].

1.6 Mechanisms

Targeting tumor cells can be done in two ways: passively and actively [87, 88].

1.6.1 Passive Targeting

To enhance nanoparticle uptake, passive targeting leverages the two primary distinctions between tumor cells and healthy cells [89]. The acidic tumor microenvironment and leaky vasculature present in these cancer cells are the main distinctions. Rapid cell growth results in leaky vascularization, wherein the nanoparticles can diffuse into the cells due to improper development of the circulatory cell walls [89]. Pro-drugs and high concentrations of targeted medications build up in tissues with a higher permeability to blood through a passive targeting mechanism that exhibits an enhanced penetration and retention impact. The increased permeability and retention (EPR) effect has been shown to raise active medication concentrations in cells with cancer by a factor of 10–100. Additionally, the microenvironment increases uptake through passive targeting.

1.6.2 Active Targeting

The acidic cytoplasm of cancer cells can be used to absorb pH-sensitive drug conjugates, which are then broken down once the cell has been infiltrated, releasing the active medication [89]. On the other hand, active targeting (Figure 2) entails functionalizing Particles containing receptors for aiming that are unique to the target cells. Nanoparticles can be functionalized in four different ways: by attaching ligands that are receptor-targeted on their surface; functionalizing these individuals with an antibodies; utilizing the characteristics of the microenvironment as triggers to release the medication from the nanoparticles; and using external stimuli as triggers [89].

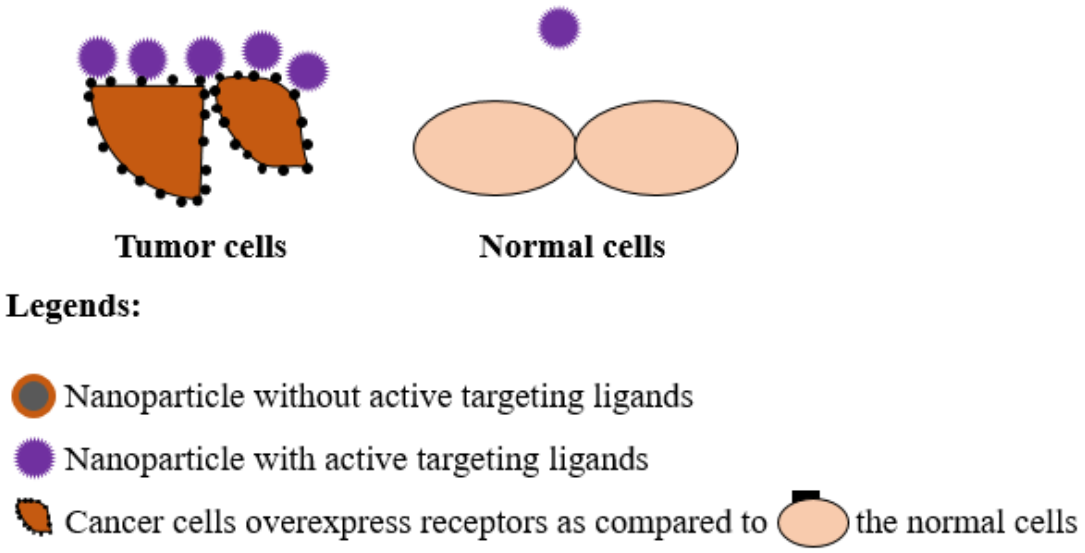

Figure 2: Diagram demonstrating that three mechanisms can achieve active targeting: covalent attachment, which occurs when a ligand is covalently bound to a particle;

passive adsorption, which occurs when a ligand binds to a particle after prolonged incubation; and biomolecular interactions, such as electromagnetic forces.

1.7 The Internalization

There are several ways for nanoparticles to enter cells, but endocytosis is the most frequent [38]. This entails the plasma membrane enclosing the nanoparticle and pinching it off to create a vesicle that contains it [90]. Three forms of endocytosis exist: receptor-mediated endocytosis, pinocytosis, and phagocytosis, which involves devouring cells.

The size and form of molecules also influences how well they are internalized into cells. According to study, spherical particles are easier to absorb than rod-like ones, while larger particles take longer to internalize [38]. Because of their size, hydrophilicity, and the vascular architecture of Compared to free medications, cancer cells selectively uptake nanoparticles [89].

1.8 Ferroptosis

Ferroptosis is a non-apoptotic process that causes cells to die on their own, according to a new research screening. The two primary features of ferroptosis—the buildup of lipid peroxides and iron dependence—set it apart from other forms of planned cell death [91]. According to recent research, ferroptosis may be used to treat cancer, particularly to eliminate aggressive malignancies that don't react to standard therapies [92]. Recent years have seen the development of anticancer medications based on ferroptosis induction. As nanotechnology has advanced in recent years, so too has the application of nanomedicine to cancer treatment. Due to their distinct capabilities and unique physicochemical characteristics, such as their electrochemical, magnetic, and photothermal effects, nanomaterials can effectively kill cancer cells. Furthermore, ferroptosis has been found to be caused by nanomaterials [93].

1.9 Applications Of Nanoparticles

There are numerous benefits of using nanoparticles as drug vesicles, including improved biocompatibility, drug molecule protection, and precise targeting, to mention a few [87, 94]. The size of drug delivery systems affects their effectiveness. Because nanoparticles are tiny and have a huge surface area, the medicine is released more quickly because it is closer to the surface. The lymphatic system is triggered and the nanoparticles are expelled from the body more quickly if they are too big, that is,

larger than 200 nm [87, 95]. The surface characteristics of nanoparticles are another feature that affects how easily they are eliminated from the body. It is possible to carefully design layer reactivity, surface curves, and targeted molecule to inhibit aggregation, boost stability, and affect receptor binding to the nanoparticles [87].

The likelihood that a nanoparticle will be eliminated from the body increases with its hydrophobicity. Their surfaces can be covered with polymers to get rid of the body's clearance [87, 95] but this doesn't stop them from aggregating. It has been claimed that the aggregation problem can be more successfully addressed by Altering the ζ-potential or applying agent caps [87, 95]. Drug release from nanoparticles can happen in two ways: either by releasing drugs that are attached to the particles' exterior or by breaking down the matrix, which releases medications from the particles' inside. This causes a brief spike in drug release followed by a sustained release [36, 87, 95, 96]. As previously said, active or passive targeting allows nanoparticles to move to their intended target once they are within the circulatory stream. To be deemed appropriate, nanoparticles need to be able to identify, bind, and deliver their load to the designated tissue while avoiding or lessening drug-induced harm to tissues that are healthy DDS.

Nanoparticles have numerous applications, most notably as a drug delivery mechanism in liver cancer cell lines. Scanning electron microscopy (SEM) elemental mapping verified the existence of iron-doped silica nanoparticles. In addition to demonstrating the absence of crystallinity in the product, X-ray diffraction (XRD) verified the existence of iron-doped silica nanoparticles. In order to increase the DDS's effectiveness and blood dispersion time, this study has since investigated a variety of characterization techniques, including silica stabilization, improved particle distribution, and tiny particle size. As a result, these characterization methods will help increase the possibility that the DDS will reach the intended or targeted tissues.

1.10 Using Nanoparticles To Deliver Drug

Nanoparticles have a lot of promise for use in drug delivery, as was previously mentioned. Current systemic drug administration techniques have several drawbacks, including as low drug vesicle stability and solubility, quick drug molecule breakdown and excretion, a lack of targeting, and undesirable side effects [31]. Among the many benefits of using nanocarriers as drug vesicles are their high level of biocompatibility, ability to protect drug molecules, and precise targeting. Chen et al. conducted one of

the earliest investigations into nanoparticles as DDS [97]. Using TEM, they created porous hollow silica nanoparticles that had an outermost layer thickness of 10 nm and a typical diameter of 60–70 nm. It was possible to regulate the nanoparticles' diameter and structure. Because they were made using calcium carbonate templates. Cefradine, an anti-cancer medication, was successfully ensnared within the nanoparticles' pores. According to a 12-hour trial, these drugs released rapidly and significantly during the first 20 minutes, then gradually and steadily over the next 10 hours [97]. It was determined from the foregoing crystalline silica nanoparticles with hollow pores may be effectively employed as DDS. Studies have shown the ability of nanoparticles to utilize encapsulate fluorescent compounds that can be employed as contrast agents or for imaging, as well as to store and release a variety of medications in a controlled manner. In order to encapsulate different molecules, silica often forms a mesoporous network with numerous empty channels [37]. Silica can be used to create nanoparticles with enormous surface areas and pore sizes, with typical diameters of about 100 nm. This results in the aforementioned beneficial characteristics as well as adjustable particle and pore diameters. Additionally, the particles' outer and inner surfaces can be functionalized (Figure 3), enabling them to function as targeting systems and drug vesicles at the same time [37]. The ability to disintegrate is necessary for the package of nanoparticles to be released in situ.

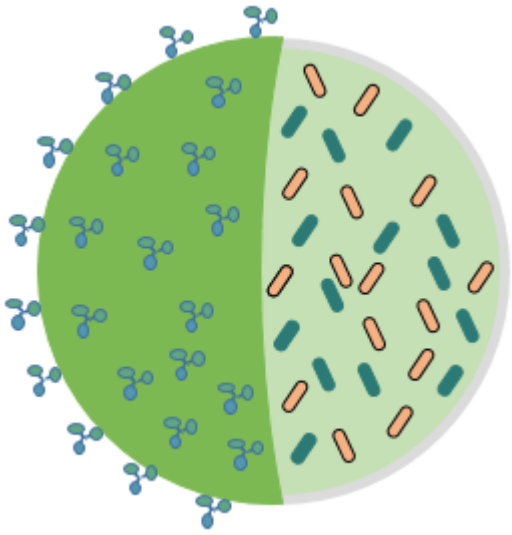

Figure 3: Schematic of a nanoparticle with drug payload enclosed and antibody-functionalized surface

1.11 Nanoparticles For The Treatment Of Cancer

Numerous medications have been put into nanoparticles for a range of therapeutic purposes since they were found to be an appropriate DDS. Anti-cancer medications are one class of medications that are extensively studied. The administration of hydrophobic anti-cancer drugs was examined in a previous study by Lu et al. in order to get around the challenge of giving poor solubility medications intravenously [98]. They produced FITC-NPs loaded with apothecia (CPT), and TEM and XRD analysis showed that the spherical nanoparticles were less than 130 nm in size. The technique of fluorescent microscopy was used to monitor cell uptake when these small fragments were treated with cancer cell types. The findings demonstrated that anti-cancer medications can be delivered and transported (Figure 4) into cells using nanoparticles with little to no medication seeping into the cultural media [98]. Lu et al. looked into the biodistribution and biocompatibility of cancer medications in mice three years later [40]. After demonstrating effective anti-cancer medication delivery and storage in vitro, they proceeded to study in vivo.

Figure 4: Diagram demonstrating a functionalized targeted silica nanoparticle with encapsulated medication Transition from epithelial to mesenchymal

1.12 Transition From Epithelium To Mesenchymal

Among the several pathogenic processes that rely on the epithelial mesenchymal transition (EMT) are the spread and invasion of tumors. During Epithelial cells undergo loss of epithelial characteristics during EMT, and instead acquire the morphological and biochemical characteristics of mesenchymal cells [99, 100]. Typical EMT malignant tumor cells have increased mesenchymal characteristics, increased motility, and invasion. They also show unregulated expression of mesenchymal marker genes and down regulated expression of cell adhesion molecules [101, 102]. EMT is essential for giving HCC its invasive and metastatic characteristics [103, 104]. Several signalling pathways are known to influence EMT, including

nuclear factor kappa-B (NF-kB), phosphatidylinositol 3-kinase/protein kinase B (PI3K/AKT), and mitogen-activated protein kinase/extracellular regulated protein kinases (MAPK/ERK) [105-107], whereby the regulation of tumor invasion and metastasis is greatly aided by the PI3K/AKT pathway. Furthermore, there are two ways in which the PI3K/AKT signalling pathway might cause EMT: growing transcription factor and matrix metalloproteinase expression a snail [108-112].

AIMS AND OBJECTIVES

Objectives of this study are:

- To control the porosity by the addition of surfactant
- To synthesize iron-doped mesoporous silica nanoparticles
- To characterize as synthesized nanoparticles
- To estimate the effect of nanoparticles on liver cancer metastasis

CHAPTER 2

LITERATURE REVIEW

2.1 Cancer

As the 2nd greatest cause of mortality in the US, cancer is an important global health problem. The 2019 coronavirus disease pandemic (COVID-19) delayed the identification of cancer and treatment because of closures of medical facilities, changes in health insurance and work, as well as anxiety over being exposed to COVID-19. Health care delivery has not entirely recovered, despite the fact that the impact was worst during the COVID-19 peak in mid-2020. For instance, Massachusetts General Hospital's surgical oncology treatments had the least amount of recovery in 2021 across all surgical specialties, recovering only 84% of their 2019 levels in the latter half of 2020. Mortality and advanced-stage disease may increase as a result of delayed diagnosis and treatment. It will take several years to quantify these and other secondary pandemic impacts at the population level because population-based cancer incidence and mortality statistics are delayed by two to three years. Nonetheless, it is already widely known that communities of color have been disproportionately affected by the pandemic, both directly and indirectly (Rebecca L. Siegel MPH et.al. 2023) [113].

2.2 Liver Cancer

Based on the pathological nature, liver cancer can be broadly classified as intrahepatic cholangiocarcinoma, hepatocellular carcinoma (HCC) (about 75%–85%), and various mixed kinds. It was identified as the third leading factor in death due to cancer globally and ranks sixth more common kind of cancer. Over half of all carcinomas of the liver cases globally occur in China, indicating significant regional variations in the disease's distribution. Given the current high prevalence of liver cancer, sensible measures that priorities primary prevention and surveillance have been developed. The central government has also implemented a number of programs to increase the number of people who have received the hepatitis B vaccine. These actions have demonstrated their effectiveness in lowering overall mortality and avoiding the onset of liver cancer. In 2020, there were an anticipated 905,677 liver cancer diagnoses globally, with an age-standardized incidence rate of 9.5 cases per 100,000. The age-standardized

incidence rate of liver cancer was 5.2 per 100,000 for women and 14.1 per 100,000 for men. The prevalence of liver cancer varies significantly by location, with transitioning regions having the highest rate.

2.3 Hepatocellular Carcinoma (HepG2)

More than 90% of instances of liver cancer are hepatocellular carcinoma (HCC), making it the most prevalent kind. About 50% of cases of HCC are caused by hepatitis B virus (HBV) infection, making it the most significant risk factor for the disease's development. Patients' sustained virological response (SVR) to antiviral medications has significantly reduced the chance of contracting the hepatitis C virus (HCV). Even after being cleared of HCV, those with cirrhosis are thought to be at a significant risk of developing HCC. The HCC aetiology with the fastest rate of increase is particularly in the West, non-alcoholic liver disease (NASH) is linked to a condition called metabolic syndrome or diabetes mellitus. Additionally, aristolochic acid and nicotine have been discovered as potential pathogenetic cofactors in HCC through investigations on mutational signatures. Although tissue biopsies are increasingly needed in clinical practice for molecular characterization of the tumor, non-invasive criteria are typically used to diagnose HCC. In terms of prevention, accumulating evidence supports the preventative effect of aspirin and coffee in addition to immunizations that prevent HBV infection and antiviral treatments for HBV and HCV infection (Josep M. Llovet et. al.2021) [114]. Surgeons, medical oncologists, radiation oncologists, and interventional radiologists should collaborate in a multidisciplinary way to provide the best care for patients with HCC. Treatment paradigms need to take into account patient-related and tumor-related aspects, such as the severity of liver disease, which contributes significantly to morbidity and mortality. Individuals with advanced disease now have longer survival times thanks to the development of more potent systemic and locoregional medicines. Additionally, some individuals who would otherwise have regarded incurable disease are now able to receive surgery (Zachary J. Brown et. al, 2023) [115].

2.4 Drug Delivery Systems (DDS)

In both experimental and clinical contexts, drug delivery systems (DDS) have been used to deliver therapeutic molecules for the treatment of illnesses. Oral ingestion or injection are the two methods used to administer conventional DDS. Even though the

traditional DDS has numerous benefits, including being simple to administer and being generally accepted by patients. Plenty of the drawbacks of traditional medicine delivery techniques can be addressed by supervised drug distribution systems. For example, the non-specific administration of chemotherapy medications damages both cancerous and natural cells, leading to their high toxicities and poor efficacy. Controlled DDSs would effectively carry chemotherapeutic chemicals to the tumor location, increasing drug concentrations in cancer cells and avoiding harm to healthy cells. Furthermore, biomolecules and cutting-edge medicinal substances like interference with RNA and gene therapy can be delivered with the help of controlled DDSs, which shield the medications from deterioration and elimination. They can assist DNA and siRNA in avoiding enzymatic breakdown and absorption by reticuloendothelial or other tissues. Since nanotechnology has advanced, nanoparticles have emerged as a viable option for regulated medication delivery systems. The term "nanoparticle" is commonly used to describe particles that have between 10 and 1000 nm in diameter. By extending the medication's half-life, making some hydrophobic drugs more soluble, and releasing the drug in a controlled or sustained manner, nanoparticles can be used as a DDS to increase the medication's effectiveness (Yu Dang, et.al.2020) [116]. Systems for delivering pharmaceuticals at the nanoscale are a crucial way to lessen side effects and increase the effectiveness of chemotherapy medications. Utilizing nanostructured materials in DDS offers unparalleled flexibility in modifying the drug's inherent qualities, including t1/2, immunogenicity, drug release characteristics, dissolution, solubility, and bioavailability. Given that many physiological processes occur at the nanoscale, another significant characteristic of nanostructured materials (NSM) is that they are about the same size as the organelles are part of the cell found in human cells. This characteristic makes NSM a viable choice for DDS. The ability of nanoparticles should have a large carrier capacity, vary in size and shape, and establish stable connections with ligands, and readily bind both hydrophilic and hydrophobic substances allows for the target-specific and controlled delivery of micro and macromolecules in disease therapy (V. Chandrakala, et.al 2022) [117].

2.5 Silica Nanoparticles

The most prevalent substance on Earth is silicon dioxide (SiO_2), also referred to as silica in common usage. In addition to being present in plants and grains, silica is

widely distributed in the Earth's crust as silicate minerals. Because silanol groups (Si–OH) are present, silica nanoparticles (SiNPs), an inorganic substance, have uniform pore sizes, adjustable particle sizes, huge surface areas, easily modifiable surfaces, and exceptional biocompatibility. These characteristics indicate that the inorganic silica skeleton is more stable than traditional drug delivery techniques in acidic conditions, organic solvents, and temperature fluctuations. SiNPs are now the second-largest nanomaterial manufactured globally due to the expansion of SiNP manufacturing. Consequently, research on SiNPs' toxicity has also grown. A type of amorphous silica nanoparticle with an irregular shape and no specific structural shape, nonporous silica nanoparticles are highly biocompatible and have a wide range of uses, such as medication transport, imaging, enzyme encapsulation, therapies (as stabilizing agents), and more. Generally speaking, there are two kinds of N-SiNPs preparation techniques (Yanmei Huang, et.al.2022) [118].

2.6 Role Of Silica Nanoparticles In Targeted Drug Delivery

The initial studies on materials made of mesoporous silica (MSMs) were published in the 1990s by researchers from Mobil Oil in the US and Kuroda et al. in Japan. In the process of creating bulk mesoporous materials, Surfactant particles that self-assemble serve as patterns for neighboring silica precursors to condense. The result of taking out the template is a substance that is filled with holes in networks. This novel substances group has a large large pore size (ca. 1 cm^3 g^{-1}), a high density of silanol groups at their surface, an ordered arrangement of pores with uniform diameters between 2 and 20 nm, and a large surface area (ca. 1000 m^2 g^{-1}).. These features could make further functionalization procedures easier. These qualities make MSMs perfect for uses that might call for molecule adsorption, like drug delivery systems, which 2001 saw the initial proposal from the Vallet–Regí group. The remarkable properties of MSNs for biological applications have led to the development of novel enhanced multifunctional materials for a variety of biotechnological applications. Among them, recent developments in biomedical research using MSNs could be some of the foundations for future highly selective diagnostic techniques and tailored treatments. The development of nanoparticles that can establish intimate connections with biological systems is thus made possible by continuous advancements in the field of nanotechnology encompassing methods for synthesis and characterization. The most

recent advancements in MSNs will be the main topic of this Progress Report. they are used in medication delivery systems (Miguel Manzano, et al., 2020) [119].

Mesoporous silica's ability to load and release medications is essential for delivering therapeutic agents for focused treatment, which maximizes efficacy. Together with their biocompatibility, adaptability, and low toxicity, these nanoparticles' special qualities allow for precise hemorrhage control, wound healing, and the activation of therapeutic molecules within injury sites. This makes them potentially useful biomaterials for hemorrhage therapy applications.

Because of their large surface area, increased pore size, and superior biocompatibility, mesoporous silica nanoparticles (MSNs) have recently become attractive options for hemorrhage control. During the hemostasis process, these features have a direct impact on the toxicity of cells, the loading of therapeutic substances, and the release of active ions. Therefore, in order to develop these kinds of carriers, it is crucial to comprehend the principles of tuning these properties. Although the function of MSNs in hemorrhage management has been examined in a number of literature reviews, in-depth research on their general traits and particular uses is still lacking (Talib M. Albayati, et.al 2024) [120].

2.7 Iron-Doped Silica Nanoparticles

Iron's bio compatibility and ability to avoid toxicity are two of the primary justifications for putting it on silica, as iron includes elements that are heavy are detrimental to biological systems. Consequently, an appropriate technique to avoid toxicity and make iron easily utilized in biological applications is to wrap it with biocompatible silica. In order to create multipurpose core/shell silica nanocomposites that conjugated with folate that enabled the fluorescence imaging of malignant cells, Fe_3O_4 magnet nanoparticles were encased within hollow silica nanospheres (Sun et al.). Water-soluble and iron-soluble Cetyltrimethylammonium bromide (CTAB)-stabilized Fe_3O_4 nanoparticles act as templates, and Tetraethylorthosilicate (TEOS) is used as a precursor to form hollow silica nanocomposites (Ali Tufani, et.al 2021) [121].

2.8 Controlling Porosity In Silica Nanoparticles

Porous silica has been among the biggest advancements in nanotechnology in recent years. Very porous silica materials have several qualities, including non-toxicity, low cost, simplicity of production, chemical inertia, and thermal stability,

biocompatibility, and good flexibility in surface functionalization. As a result, professionals worldwide have focused a lot of emphasis on using this porous silica in a variety of applications, including medication delivery, optically active materials, energy application, sensing, and catalysis. The most common methods for producing mesoporous silica are either using quaternary alkyl ammonium surfactants, like CTAB, as a template in extremely basic circumstances or triblock copolymers under extremely acidic conditions, such as Pluronic F127, P123, etc. The supramolecular self-assembly of the surfactants (or templates) is the essential basis of all syntheses, notwithstanding considerable variance in the porous silica's geometry and synthesized circumstances. Organic–inorganic silica–template composites are created in alkaline or acidic environments, hydrolyzed inorganic silica precursors, including, TEOS, cluster surrounding these templates the micelles. Cooperative Organic surfactant particles self-assemble by taking place in the solution phase at levels greater than the miceller's critical concentration (CMC) (Nabanita Pal, et al. 2020) [122]. TEOS is the main silica precursor used in the surfactant-templating method and surfactant molecules (such as CTAB) as structure-directing templates, is used to generate ordered mesoporous silica species. It is possible to draw conclusions from general particle formation concepts even while the process of MSN generation is not compelling. In a generalized process of MSN generation, the extra surfactant molecules in the alkalescent media first systematically self-assemble into micelles at their critical micelle concentration (CMC) (Ranjith Kumar Kankala et al., 2020) [123].

The atrane approach, a previously published "one-pot" method, was used to synthesize hierarchically structured mesoporous silica. The molar ratio 2 − n Si: n Fe: 7 TEA: 0.5 CTAB: 180 H_2O was preserved in all situations where the CTAB surfactant was used to create solids with (2 − n)/n = X = 100, 50, 25, and 10. The iron concentration of the obtained samples led to its designation as FeX-UVM-7-C16. Thus, in a standard synthesis (Fe50-UVM-7-C16), 23 mL of TEA, 11 mL of TEOS, and 0.19 g of $FeCl_2$•$4H_2O$ were mixed together and heated to 140 °C until a homogeneous solution was obtained. The solution was allowed to cool to 120 °C before 4.68 g of CTAB surfactant was added and swirled. 80 mL of ultrapure water at 85 °C is the last step. After adding water, the mixture was vigorously agitated overnight at room temperature. Vacuum filtration was used to collect the resulting solid, which was then gently washed with ethanol and water. After that, the solid was left to air dry before

being dried at 80 °C in an oven. The mixture was calcined at 550 °C for six hours to eliminate the surfactant, yielding the final product (Enric Pellicer-Castell et al., 2022) [124].

2.9 Loading Drug On SiO_2 Nanoparticles

Sorafenib-loaded IONPs were created by dissolving 5 mg of nanocomposites with various SO concentrations (5, 10, 20, 40, 80, and 120 mg/mL) in 5 mL of acetone. The liquids were then ultrasonically agitated for 30 minutes. After being dried at 70 °C, the collected specimens were rehydrated at 80 °C using 5 mL of phosphate-buffered saline (PBS). Following a half-hour incubation period, the drug-encapsulated IONP-SiO_2 nanocomposites sites (IONP-SiO_2-SO) were centrifuged at 19,000 rpm for 15 minutes. The resultant solid products were then immediately employed after being cleaned using a new, ice-cold aqueous buffer (pH = 7.4) (Ndumiso Vukile Mdlovua et al., 2020) [125].

CHAPTER 3

METHODOLOGY

3.1 Apparatus

Hot plate, ice bath, round bottom flask, magnetic stirrer, thermometer, iron and tripod stand, centrifuge machine, autoclave or hydrothermal reactor, heating furnace and other usual laboratory glassware's

3.2 Chemicals

From Sigma Aldrich, we acquired $FeCl_3.6H_2O$ (iron chloride hexahydrate, 99%), NaOH (sodium hydroxide, 99%), sodium dodecyl sulphate (SDS), diquaternary ammonium salt (DA), tetraethyl orthosilicate (TEOS, 99.9%), hydrochloric acid (HCl, approximately 37%), and surfactant (cetyltrimethylammonium bromide (CTAB, 98%). The top-notch university lab produced ethanol and deionized water. Sigma Aldrich provided the MTT, HepG2, and sorafenib tosylate (SO). Every chemical and reagent utilized in the studies was of analytical grade.

3.3 Iron-Doped Silica Nanoparticle Synthesis Using Different Surfactants

The iron-doped silica nanoparticles were created using a previously published one-pot process, which was modified somewhat from that publication [126]. 20 mL of 1M NaOH solution was added while stirring at room temperature after the surfactant (CTAB 9.94 mmol, SDS 47.85 mmol, and DA 0.859 mmol) above the CMC value dissolved in deionized water (60 mL) mixture and 399.96 mmol of TEOS. Solution was treated with iron chloride 40.04 mmol for 24 hours at pH 11. After this period, the suspension was treated with 1 M hydrochloric acid to lower its pH to 7. Centrifugation was used to collect the yellowish-white precipitates, which were then cleaned twice with ethanol and deionized water before being dried for a whole night at 70 °C in oven. The solid materials were calcined at 600 °C for four hours with airflow (100 mL min^{-1}) in an electric furnace to eliminate the surfactant [127]. FeMS(C), FeMS(S), and FeMS(DA) nanoparticles were assigned to this sample.

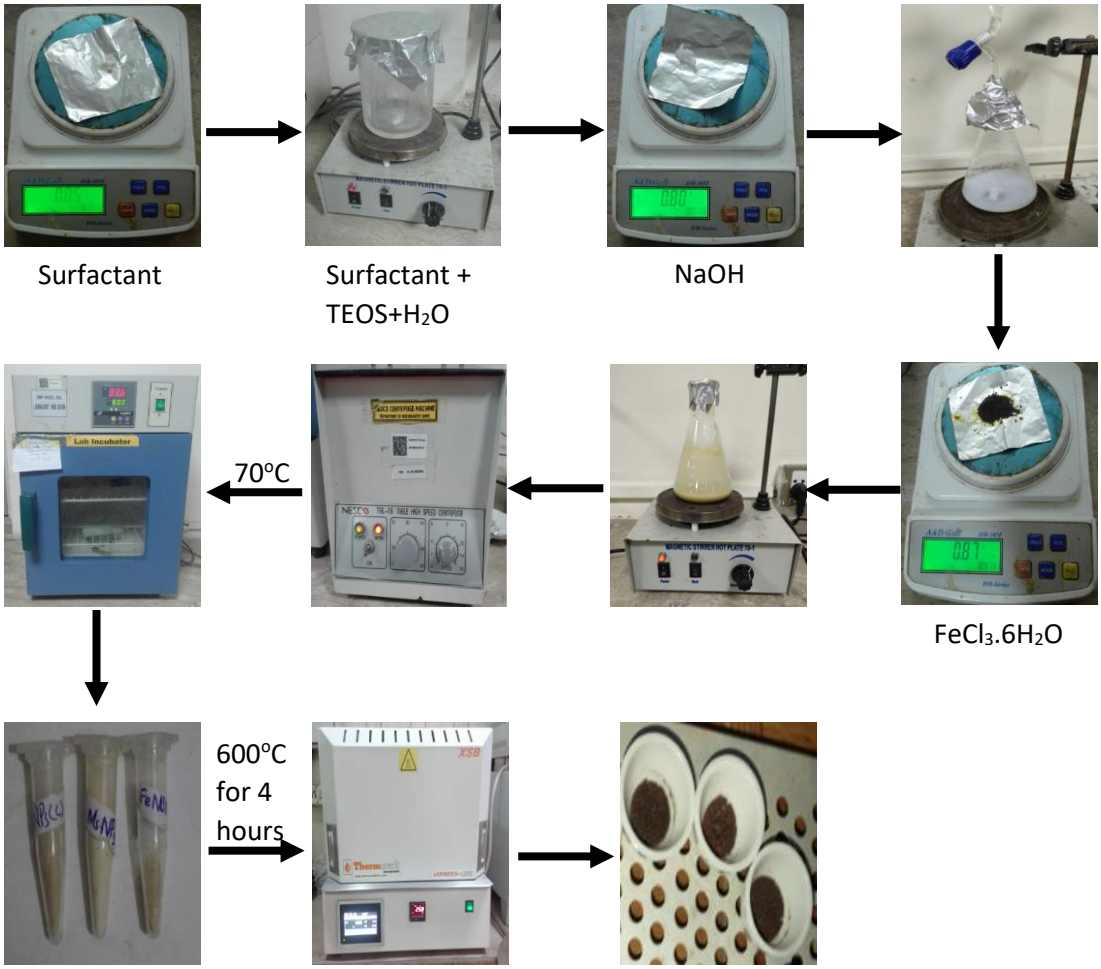

Figure 3.1 Synthesis of FeMS(C), FeMS(S), and FeMS(DA) nanoparticles via one-pot method

3.3 Identification Of The Properties Of Iron-Doped Silica Nanoparticles

Pilot high-resolution image of iron-doped silica nanoparticles in solution with the help of SEM. Similarly, monochromatic CuKa radiation was used to guide the objects' X-ray diffraction (XRD) patterns. Different functional groups identification was carried out by FT-IR, the successful coating of iron was verified. Determining the pore volume and size distribution of iron-doped silica nanoparticles—all critical parameters for a variety of applications—requires the BET characterization of these particles. Thermogravimetric analysis (TGA) in iron-doped silica nanoparticles helps determine thermal stability and decomposition behavior, and assess the effectiveness of the silica coating.

3.4 Drug Encapsulation

The nanoparticles were further loaded with sorafenib for tumor therapy. The SO-encapsulated iron-doped silica nanoparticles used in this study were prepared with minor modifications from previous studies [125, 128]. To prepare SO solution, 40 mg sorafenib dissolved in 20 mL phosphate buffered saline (PBS). 40 mg nanoparticles were added in SO solution and prepared drug loaded nanoparticles (FeMS(C)-SO, FeMS(S)-SO, and FeMS(DA)-SO). FeMS(C)-SO, FeMS(S)-SO, and FeMS(DA)-SO, the drug-encapsulated iron-doped silica nanoparticles, were centrifuged for ten minutes at 4,000 rpm. A UV-VIS spectrophotometer set to 240 nm was used to measure the SO content in the supernatant solution.

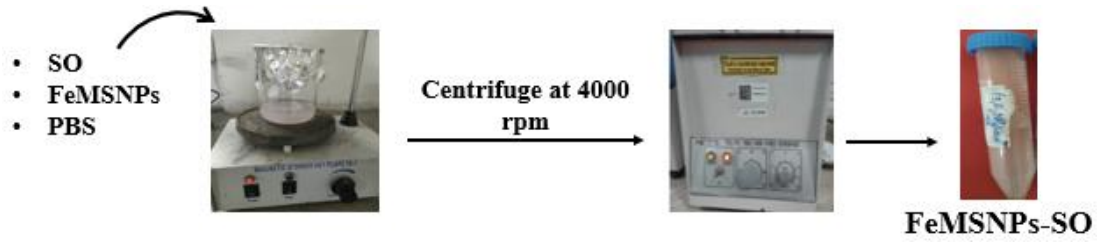

Figure 3.2: Drug sorafenib loaded on different nanoparticles (FeMS(C), FeMS(S), and FeMS(DA) → FeMSNPs)

3.5 Efficiency Of Loading

A portion of the total SO concentration used to load onto iron-doped silica nanoparticles is left unattached [129]. After centrifugation (using an Eppendorf centrifuge 5430R) for five minute at 4000 rpm, separated supernatant to remove unloaded medication. UV-Vis spectrophotometry was used to measure the amount of free SO present in the supernatant at 240 nm. The following formula (1) was used to determine the percentage of medication loading efficiency.

$$\text{DLE} = \frac{\text{Theoretical yield of drug loaded} - \text{Free drug}}{\text{Theoretical yield of drug loaded}} \text{ X } 100 \qquad (1)$$

3.6 Drug Desorption

Drug-loaded nanocomposites weighing 6 mg were suspended in 6 mL PBS buffer solutions with a pH of 7.4 and put in an orbital shaker set at 300 rpm and 37 °C in order to measure the loaded SO. Following predetermined incubation times of 15, 30, 60, 120, and 1440 minutes, the samples were removed for examination. NPs loaded with sorafenib were centrifuged for 15 minutes at 4,000 rpm at the predetermined intervals following incubation. After being resuspended in 6 milliliters of new PBS

solution, the pellet was returned to the shaker. This procedure was carried out again while keeping time in mind. By measuring the supernatant of NPs-SO at various intervals of time, SO emitted investigated. Supernatant absorbance were calculated by UV-Vis spectroscopy at 250 nm in order to quantify the amount of SO that was emitted [130, 131]. The percentage of drug loading and release was shown in table 3.1.

Table 3.1 Drug release and loading percentage on nanoparticles

Sample name	Drug loading	Sample	Drug release time (minutes)	Drug release % FeMS(C)-SO	Drug release % FeMS(S)-SO	Drug release % FeMS(DA)-SO
FeMS(C)	98%	FeMS(C)-SO	15	75%	80%	95%
			30	10%	11%	3%
FeMS(S)	92%	FeMS(S)-SO	60	7%	5%	1%
			120	5%	3%	0.5%
FeMS(DA)	80%	FeMS(DA)-SO	1440	3%	1%	0.5%

3.8 In-Vitro Cytotoxicity Studies

Using an MTT-based colorimetric test, the cytotoxic potentials of drugs, nanoparticles, and drug-loaded nanoparticles against HepG2 cells (1 × 104 cells/well) were determined at two distinct time periods (24 and 48 h) [129].

3.9 Cell-Culture

The cancer cells of human liver HepG2 with 5% CO_2 were kept at 37 °C in an incubator using DMEM (Dulbecco modified eagle medium) 10% FBS supplemented, 2 millimol per litter of L-glut, 1 milligram per milliliter of streptomycin, and 1 IU per milliliter penicillin [132].

3.10 Morphology Analysis

After 24 hours exposed the cells to the required concentration of iron-doped silica nanoparticles, they were examined by a camera system (Nikon ELWD 0.3/OD75) of the microscope fitted (Nikon Eclipse TS100) to check for any morphological changes.

Trypane blue staining was used to count the cells using a hemocytometer to determine the cell number [133, 134].

3.11 Assays For Cell Proliferation

In 96-well plates, were grown cells of 1x103 cells per well (density). Following induction by iron-doped silica nanoparticles, various tests were run to assess alterations in the viability, proliferation, and metabolism of cells.

3.12 MTT Assays

Cell metabolic activity was estimated using the MTT test. In order to conduct the MTT experiment, cells were incubated for three hours after being treated with 0.1 milligram per milliliter Thermo Fisher Scientific-M6494 (MTT salt) in Phosphate buffer saline. After adding the DMSO solution DMSO, at 570 nm absorbance was measured using the absorbance reader (BioTek EL*808) [135].

3.13 Neutral Red Assays

Cells were diluted in DMEM to a last con. of 40 microgram per milliliter neutral red for the Neutral assay, and they were then incubated for an hour. Afterwards de-staining through a 50% solution of ethanol, 49% DI H_2O, and 1% CH_3COOH (glacial acetic acid), at 570 nm absorbance measured.

3.14 Semi-Quantitative RT-PCR And RNA Isolation For Genes Associated With E-Cad, N-Cad, Vimentin, Slit-2, Integrin, And CDC42

Each liver sample's total RNA was extracted using Trizol, and oligo-(dT) was used to create cDNAs from the total RNA as previously explained. The PCR primers and profile that were used [133]. The 94 ^oC standard PCR profile for one minute, 1 minute annealing temperature, and for one minute at 72 ^oC. The cycles numbers varied aimed at each amplified gene. Under these conditions, the semi-quantitative RT-PCR tests were optimized, and the amount of each RT-PCR product was precisely proportionate to the amount of template RNA. An image analyzer was used to measure the signal intensities of products amplified by electrophoresis separated on an agarose gel (1.5%) and envisaged following gel staining of ethidium bromide. Internal oversight all samples were subjected to GAPDH RTPCR at the same time. The representative results of each RT-PCR, which was performed three times independently using different RNA preparations, are represented by the ratio of the intensity of each individual mRNA to that of the GAPDH mRNA for each sample [136].

3.15 Analysis Of Statistics

At least three cell cultures from two to three distinct passages were used to collect all of the data that was shown. The mean standard error (SEM) is used for all values. The paired t-test was used for statistical analysis. ImageJ, Prism GraphPad 7 (GraphPad Software), and Origin 2016 (OriginLab). For data and statistical analysis, software was utilized [137].

CHAPTER 4

RESULTS

4.1 Structural Techniques

4.1.1 FT-IR (Fourier Transform Infrared Spectroscopy)

Fig. 4.1 displayed the results of the FTIR examination of the FeMS(C), FeMS(S), and FeMS(DA) nanoparticles. The IR band at 631 cm^{-1} indicated the presence of Fe3O4 in FeMS(C), FeMS(S), and FeMS(DA) nanoparticles, which is caused by the stretching vibration of Fe-O-Fe [138]. Bending and symmetric stretching vibration of Si-O-Si are represented by the characteristic peak at 785 cm^{-1} [139]. Peaks at 913 and 1097 cm^{-1} were represent the Si-O-H extension and Si-O-Si asymmetric vibrations [140]. Band at 1190 cm^{-1} which show the Si-O-H stretching vibrations [138].

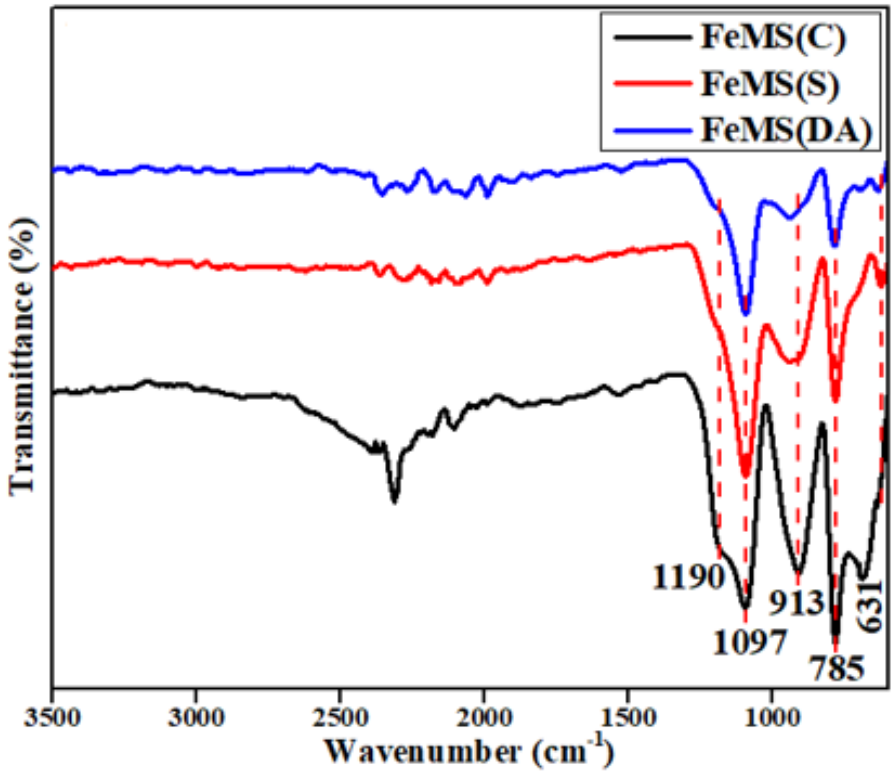

Figure 4.1 FT-IR spectra of nanoparticles

4.1.2 X-Ray Diffraction (XRD)

FeMS(C) structure was analyzed by XRD spectroscopy as shown in figure 4.2 and following characteristics peaks were appeared at 2Θ = 22.58 (021), 36.64 (220), 38.24 (221), 44.52 (033), 64.44 (401), 77.45 (171) and 81.85 (442), which are well indexed with JCPDS database (96-900-1422). Furthermore, the presence of amorphous SiO_2 in the coated layer was attributed to the broad peak that emerged in the 18°–28° range. XRD data indicates the successful inclusion of Fe_3O_4 in silica NPs, and data was used to calculate the crystallite size 13.02 nm of FeMS(C) nanoparticles using the Scherrer's equation [139, 141].

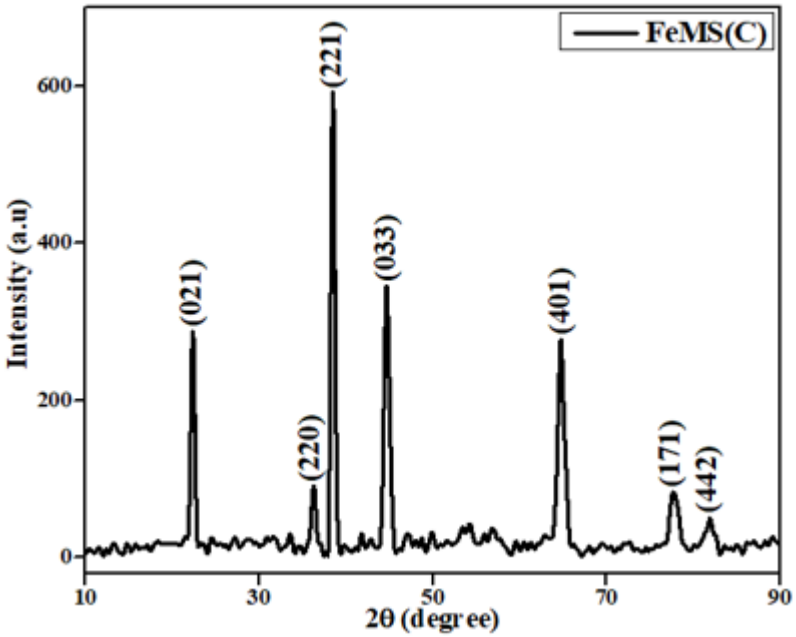

Figure 4.2 XRD of iron doped silica nanoparticles (CTAB)

4.1.3 Brunauer-Emmett-Teller (BET)

Using the BET model, the N_2 absorption-desorption method was used to determine the surface areas in the low-pressure range. For FeMS(C), FeMS(S), and FeMS(DA) nanoparticles synthesized by a co-precipitation technique, the observed BET surface areas are 189.85, 194.86, and 263.76 m^2/g, respectively (given in Table 4.1). Therefore, increasing the surface area is justified by decreasing the particle's size [142-144].

Table 4.1 Characterization parameters of different nanoparticles

Sample	BJH*			BET (m^2/g)	Langmuir
	Surface area (m^2/g)	Pore size (nm)	Pore volume (cm^3/g)	Surface area (m^2/g)	Surface area (m^2/g)
FeMS(DA)	119.77	51.97	0.2467	189.85	-
FeMS(S)	103.42	52.73	0.2569	194.86	223.12
FeMS(C)	131.04	52.14	0.3437	263.76	303.70

4.2 Morphological Technique

4.2.1 SEM (Scanning Electron Microscopy) Analysis

The nanoparticles morphology, which were described by scanning electron microscopy (SEM), is displayed in Figure 4.3 (a) and (b). The smooth surfaces of FeMS(C) and FeMS(S) resulted from the SiO_2 coating applied on magnetic Fe_3O_4 nanoparticles. The crystalline structure of magnetic Fe_3O_4 nanoparticles is uneven. Because of their small size and magnetism, surface morphology study shows that many ultrafine particles aggregate. Iron oxide particles are attached to the porous surface and these particles are in the form of pointed needles. It has a porous structure and iron oxide has accumulated inside it, which means that the iron oxide has not become part of the structure, rather, it has come separately and accumulated on the surface of the silica.

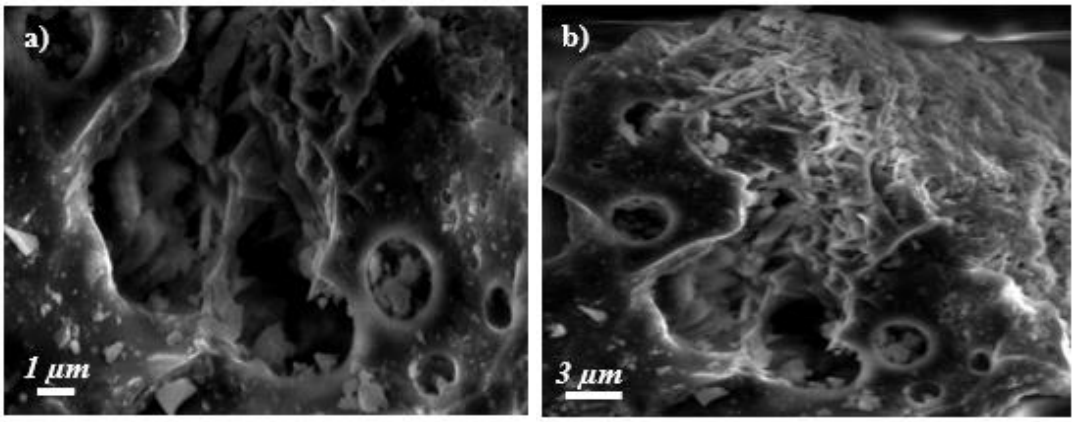

Figure 4.3 FeMS(C) and FeMS(S) scanning electron microscopy (SEM) images

4.3 Material Technique

4.3.1 Analysis of Thermogravimetric Data (TGA)

TGA was carried out at temperature range of 0.0-800.0 °C (rate of 5 °C min^{-1}). Three temperature-ranging zones make up the TGA (Figure 4.4 (a), (b), and (c)), which is represented by the black line. Water or solvent molecules being physically absorbed on the nanocomposite surface were responsible for the reported mass losses of 3.85% in FeMS(DA), 5.56% in FeMS(C), and 5.61% in FeMS(S). The desorption of small molecules caused a mass loss of 7.27% FeMS(DA), 4.52% FeMS(C), and 7.82% FeMS(S), whereas the stability of FeMS nanoparticles caused a mass loss of 6.55% FeMS(DA), 6.98% FeMS(C), and 3.48% FeMS(S). The temperature of the peaks in figure 4.4 (a), (b), and (c) can be inferred from the red line, which represents the derivative weight loss percentage [142, 143, 145].

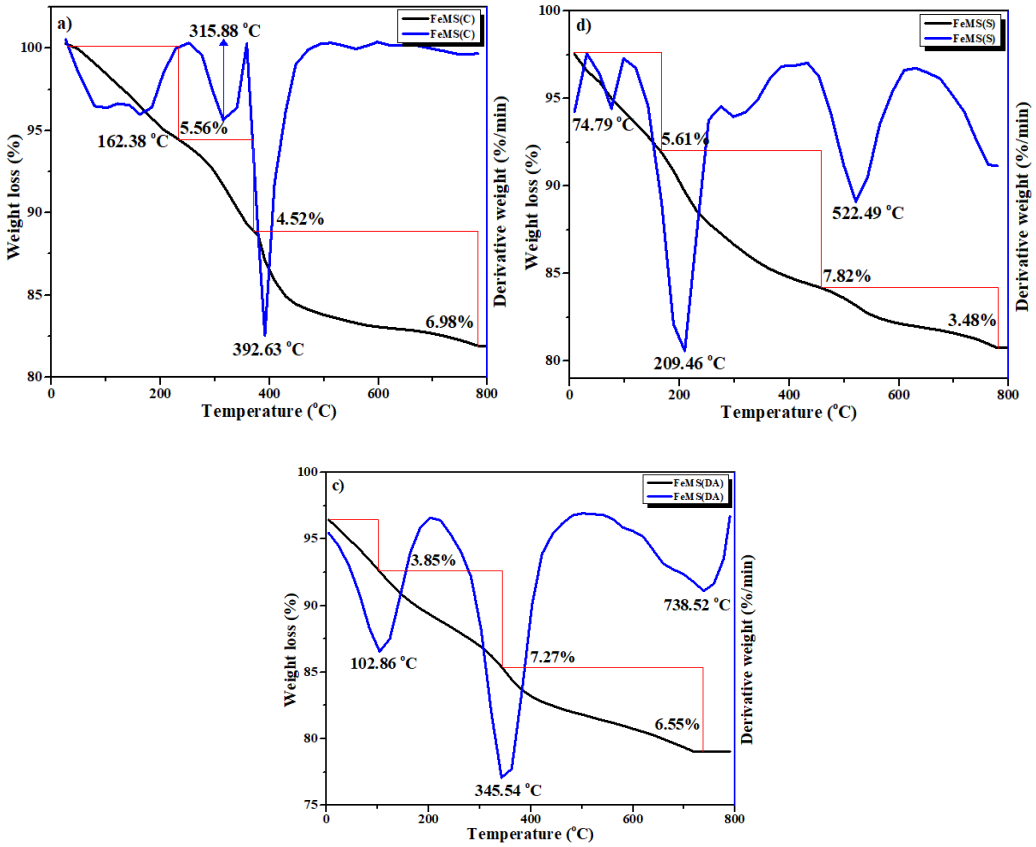

Figure 4.4 TGA/DTA spectra of (a) FeMS(C), (b) FeMS(S), and (c) FeMS(DA)

4.4 Drug Loading And Encapsulation Efficiency

UV-Vis spectrophotometer set at 240 nm was used to examine the interactions between SO and FeMS(C), FeMS(S), and FeMS(DA) nanoparticles. The absorption peak showed that SO was noncovalently loaded onto the nanoparticles (Figure 4.5) [125, 128, 129].

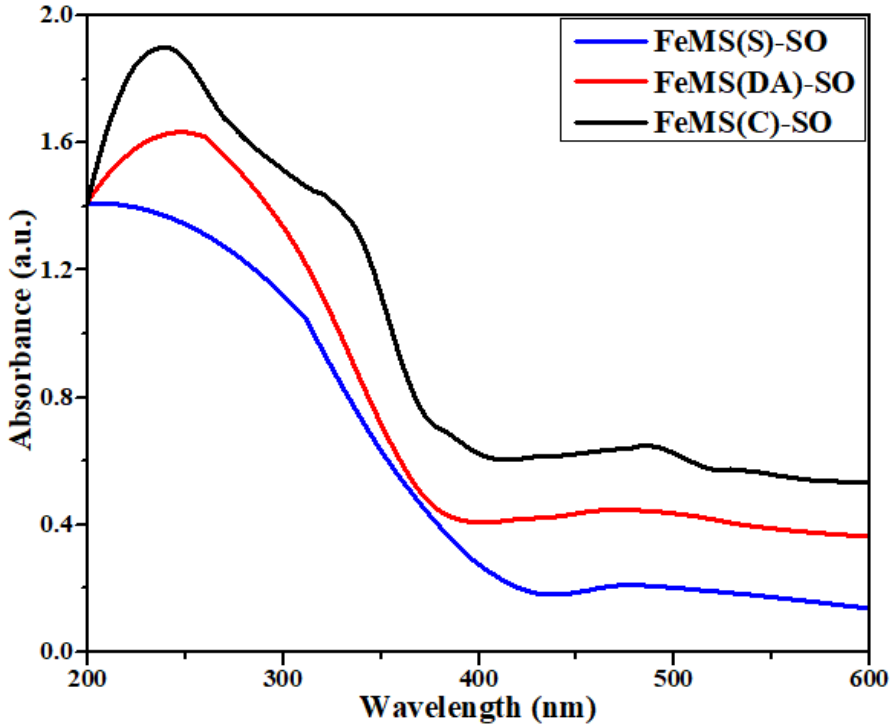

Figure 4.5 UV-Vis spectrum of drug loaded nanoparticles.

4.5 In Vitro Release Studies

At various time intervals, the release of SO from FeMS(C)-SO, FeMS(S)-SO, and FeMS(DA)-SO in 0.1 M PBS (pH 7.4) was examined (Figure 4.6). UV-Vis spectrum was used to calculate absorbance of supernatant at 250 nm in order to quantify the amount of SO that was emitted [130, 131].

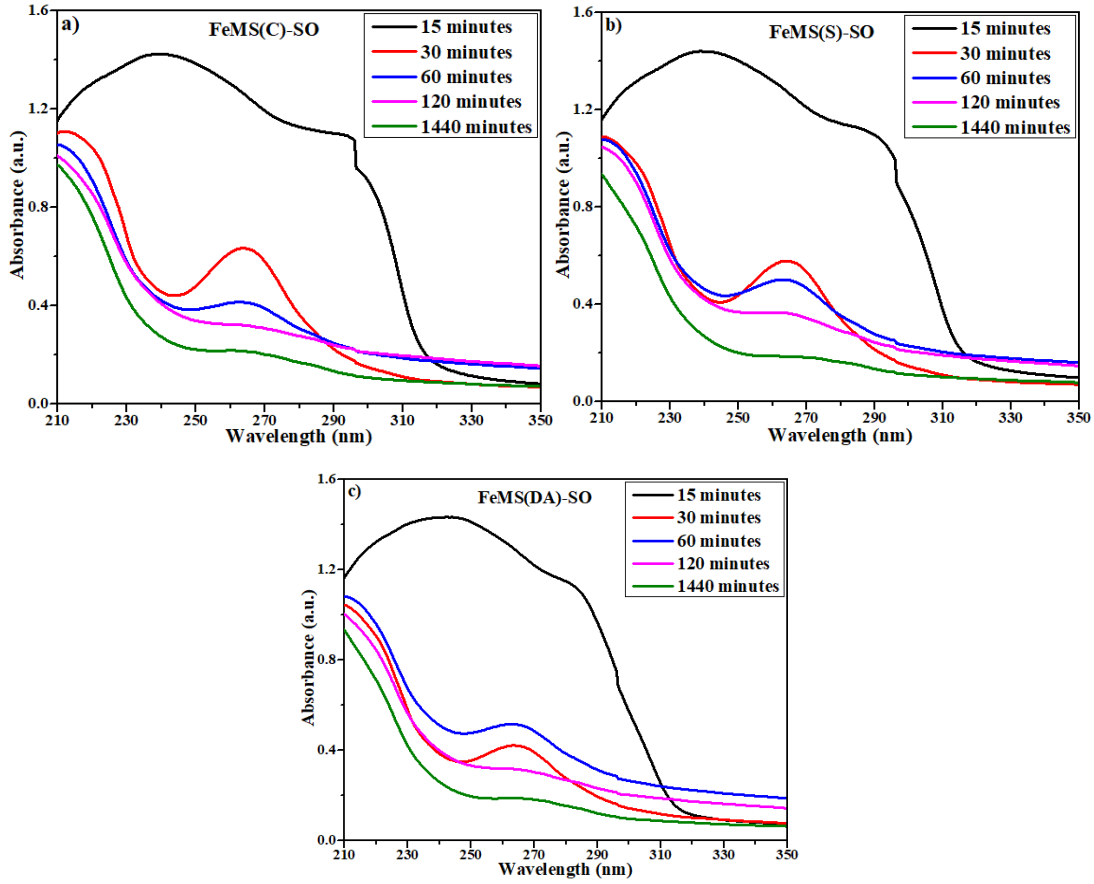

Figure 4.6 UV-Vis spectra of drug release.

4.6 In Vitro Cytotoxicity

Hepatocellular carcinoma cells (HepG2) was subjected to varying doses of free SO, FeMS(c), FeMS(S), FeMS(DA), or FeMS(C)-SO, FeMS(s)-SO, and FeMS(DA)-SO in order to assess the cytotoxicity of the formulations. HepG2 survival rates declined as FeMS(c), FeMS(S), and FeMS(DA) concentrations higher. When the quantity of Fe exceeded 1 μg/mL, the cytotoxicity of FeMS(c), FeMS(S), and FeMS(DA) against HepG2 cells was generally greater. This may be explained by the tumor cells' high GSH content, which may encourage the breakdown of FeMS(c), FeMS(S), and FeMS(DA). When FeMS(c), FeMS(S), and FeMS(DA) degrade, intracellular GSH is depleted, which causes HepG2 cells to undergo ferroptosis. The Fe concentration of FeMSNPs was 22.29±6.37 μg/mL, which is the value of IC50. GSH levels in tumor cell is typically 5 to 10 times greater as compared to those cells that are normal, ranging from 2 to 10 mM. As a result, normal cells were less susceptible to the

ferroptosis-inducing effects of FeMS(c), FeMS(S), and FeMS(DA) than tumor cells. HepG2 had reduced survival rates following loading with SO than did FeMS(c), FeMS(S), and FeMS(DA) at the same concentration. Because GSH production may be further inhibited by SO. Similarly the IC50 value 7.82±1.99 µg/mL of free SO, the IC50 values of FeMS(C)-SO, FeMS(s)-SO, and FeMS(DA)-SO were 8.3±3.99 µg/mL (Fe concentration). Stated differently, a low concentration of SO may have a greater anti-tumor effect than FeMS(c), FeMS(S), and FeMS(DA). This result is important for anti-cancer treatment due to less SO may lead to fewer side effects. Due to the fact that the FeMS(C)-SO, FeMS(s)-SO, and FeMS(DA)-SO would release components of SO that prevented cell development. Thus, additional changes are required to minimize needless medication release [146].

4.7 MTT Assays

Cell metabolic activity was estimated using the MTT test. In order to conduct the MTT experiment, cells were incubated for three hours after being treated with Thermo Fisher Scientific-M6494 (MTT salt) in Phosphate buffer saline. Then adding the DMSO solution, at 570 nm absorbance was measured using the absorbance reader (BioTek EL*808) [135].

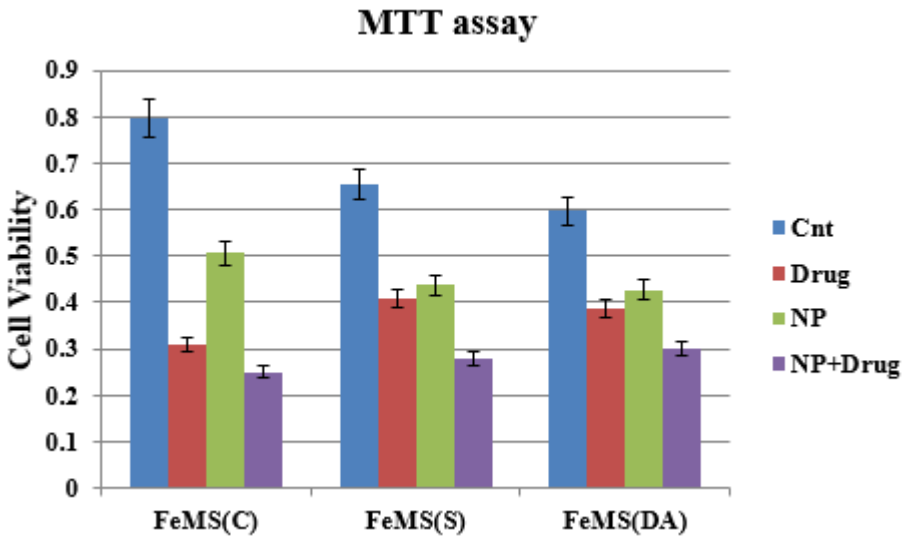

Figure 4.7 In vitro MTT assay (cell viability) of Sorafenib, iron doped silica nanoparticles, and drug loaded nanoparticles

4.8 Neutral Red Assays

Cells were diluted in DMEM for the Neutral red assay, and they were then incubated for an hour. Afterwards de-staining through a 50% solution of ethanol, 49% DI H_2O, and 1% CH_3COOH (glacial acetic acid), at 570 nm absorbance measured.

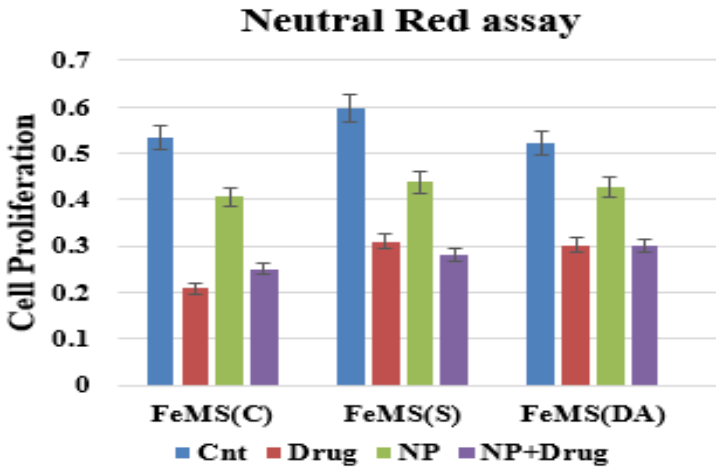

Figure 4.8 In vitro Cell proliferation test of drug, nanoparticles, and drug loaded nanoparticles

4.9 Slit2

The expression of Slit2 was checked in sorafenib and sorafenib loaded nanoparticles (FeMS(C)-SO, FeMS(S)-SO, and FeMS(DA)-SO). Expression of Slit2 in the presence of SO was less as compared to treated with the sorafenib loaded FeMS(DA), SO loaded FeMS(C), and SO loaded FeMS(S). The expression of Slit2 gene was highest in SO loaded FeMS(C) as compared to the SO loaded FeMS(S) and expression of gene was high in SO loaded FeMS(S) as compared to the SO loaded FeMS(DA).

4.10 Vimentin

The expression of vimentin gene was checked in sorafenib and sorafenib loaded nanoparticles (FeMS(C)-SO, FeMS(S)-SO, and FeMS(DA)-SO). The expression of vimentin in the presence of drug was less as compared to treat with the sorafenib loaded FeMS(DA) and SO loaded FeMS(C). The gene expression in SO was more as compared to the SO loaded FeMS(S). The expression of vimentin gene was highest in

SO loaded FeMS(C) as compared to the SO loaded FeMS(DA) and SO loaded FeMS(S).

4.11 Integrin

The expression of integrin gene was checked in the sorafenib and sorafenib loaded nanoparticles (FeMS(C)-SO, FeMS(S)-SO, and FeMS(DA)-SO). The expression of integrin in the presence of SO was more as compared to when treated with the sorafenib loaded FeMS(DA). The SO expression was less as compared to the SO loaded FeMS(C) and SO loaded FeMS(S). The expression of integrin gene was highest in SO loaded FeMS(S) as compared to the SO loaded FeMS(C) and SO loaded FeMS(DA).

4.12 CDC42

The expression of CDC42 gene was checked in sorafenib and sorafenib loaded nanoparticles (FeMS(C)-SO, FeMS(S)-SO, and FeMS(DA)-SO). The CDC42 expression in SO was less as compared to treated with the sorafenib loaded FeMS(DA), SO loaded FeMS(C), and SO loaded FeMS(S). The expression of gene in SO loaded FeMS(S) was higher to the SO loaded FeMS(C). The SO-loaded FeMS(C) was high than the SO loaded FeMS(DA).

4.13 N-Cadherin

The expression of N-Cadherin gene was checked in sorafenib and sorafenib loaded nanoparticles (FeMS(C)-SO, FeMS(S)-SO, and FeMS(DA)-SO). The expression of N-Cad in the presence of SO was equal as compared to treated with the sorafenib loaded FeMS(DA) and SO loaded FeMS(C). The gene expression in SO was less as compared to the SO loaded FeMS(S). The expression of N-Cad gene was highest in SO loaded FeMS(S) as compared to the SO loaded FeMS(C) and SO loaded FeMS(DA).

4.14 E-Cadherin

The expression of E-Cadherin gene was checked in sorafenib and sorafenib loaded nanoparticles (FeMS(C)-SO, FeMS(S)-SO, and FeMS(DA)-SO). The expression of E-Cad in the presence of SO was equal as compared to treated with the sorafenib loaded FeMS(DA) and SO loaded FeMS(C). The gene expression in SO was more as compared to the SO loaded FeMS(S). The expression of E-Cad gene was lowest in SO loaded FeMS(S) as compared to the SO loaded FeMS(C) and SO loaded FeMS(DA). Overall the expression of E-Cad was less as compared to the N-Cad it means that cancer spread.

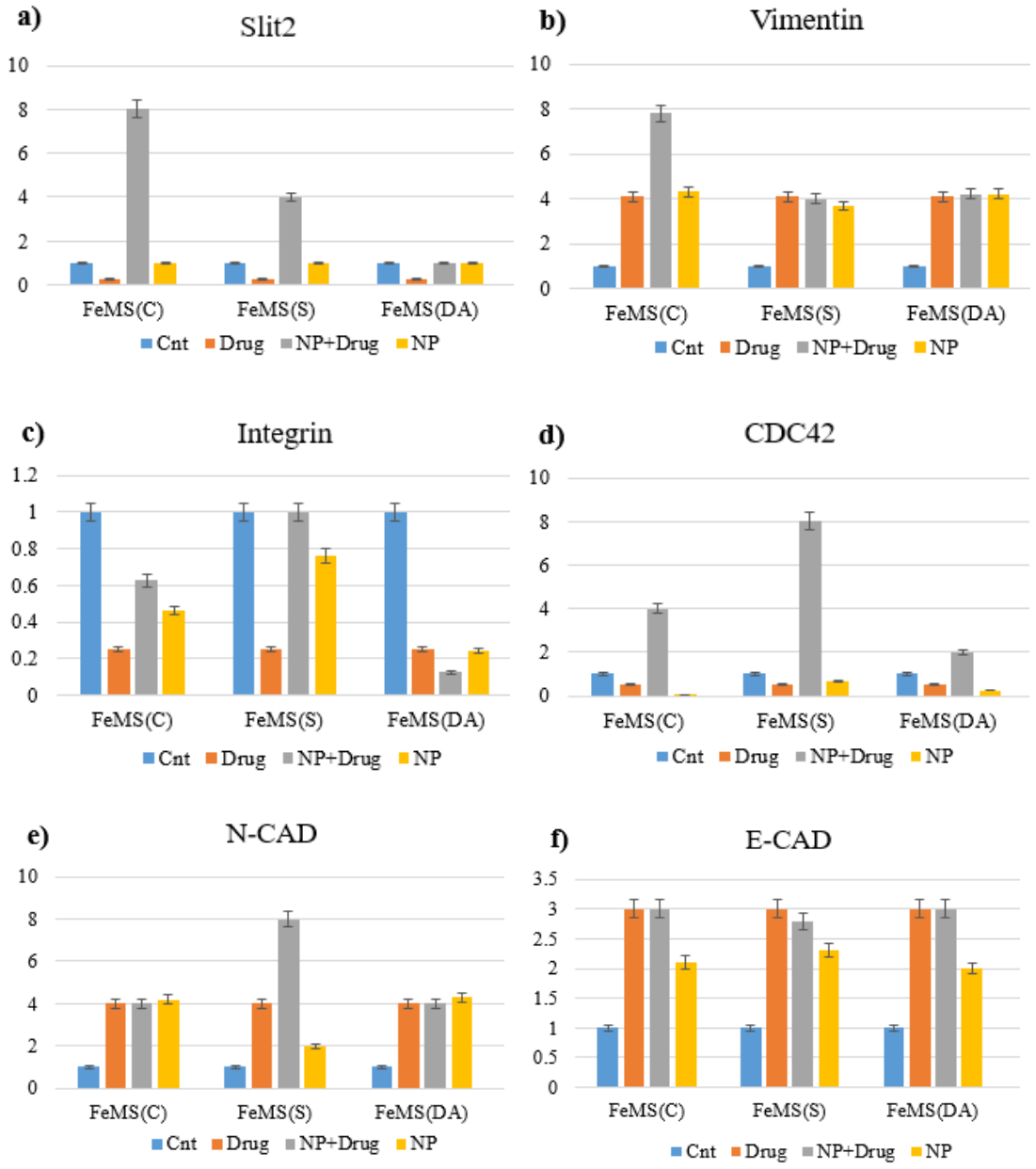

Figure 4.9 Effect of durg, drug loaded nanoparticles and nanoparticles on different genes

CHAPTER 5

DISCUSSION

Iron-doped mesoporous silica nanoparticles (FeMS) were synthesized using three distinct surfactants—CTAB, SDS, and dopamine (DA)—in order to adjust porosity and assess their suitability as sorafenib drug carriers for liver cancer treatment. The synthesis technique successfully produced three series of nanoparticles, FeMS(C), FeMS(S), and FeMS(DA), which were then thoroughly characterized using FT-IR, XRD, SEM, TGA, and BET measurements. With surfactant type having a significant impact on surface area and pore architecture, these characterization techniques confirmed the production of well-organized, porous, and thermally stable mesoporous materials. These findings are consistent with earlier studies showing how important surfactants are in determining mesostructure and drug-loading effectiveness. Remarkably, FeMS(DA) displayed greater surface area and more effective dispersion, which may be related to dopamine's dual function as a structural modifier and chelating agent, as reported in studies on its use in expanding mesoporous frameworks. All of the FeMS(C)-SO, FeMS(S)-SO, and FeMS(DA)-SO nanoparticle variations showed excellent sorafenib encapsulation when drug loaded. However, due to its more homogenous mesostructure and reduced pore size distribution, FeMS(DA)-SO demonstrated the best regulated and prolonged drug release profile. Drug-loaded nanoparticles showed great therapeutic promise in in vitro tests employing HepG2 liver cancer cells. Gene expression profiling showed downregulation of mesenchyme markers N-cad, vimentin and CDC42 and overexpression of epithelium marker E-cad, indicating effective suppression of the epithelial-to-mesenchymal transition (EMT). Remarkably, these EMT-related genes were most modulated by the FeMS(DA)-SO nanoparticles, which is consistent with the reported drug release pattern and cellular uptake values. Despite the fact that these findings confirm the effectiveness of FeMS(DA)-SO as a targeted delivery system for the treatment of liver cancer, several surprising findings were discovered. FeMS(S)-SO, for instance, showed somewhat lower drug loading and less effective gene modulation, which may be the consequence of SDS templating causing a decrease in structural integrity or a less desirable pore

structure. These results suggest that the surfactant can influence drug delivery kinetics and cell contact in addition to controlling porosity.

CONCLUSIONS

In order to control porosity and improve drug administration, this study demonstrated the efficient synthesis and characterization of iron-doped mesoporous silica nanoparticles (FeMS) using several surfactants, including dopamine, SDS, and CTAB. Sorafenib was successfully loaded into the nanoparticles, and their structural and functional properties were thoroughly examined. FeMS(DA)-SO had the most desirable characteristics of the three formulations, including a regulated release profile, enhanced drug loading capacity, and monodispersed pore distribution. The therapeutic effectiveness of the sorafenib-loaded nanoparticles was confirmed by in vitro tests using HepG2 liver cancer cell lines. By significantly downregulating mesenchyme markers (CDC42, the N-cad, Slit-2) and upregulating the epithelium marker E-cadherin, FeMS(DA)-SO demonstrated the highest anticancer action. These patterns of gene expression prevent the EMT, which is a crucial stage in the initiation and progression of cancer.

REFERENCES

1. Torre LA, Bray F, Siegel RL, Ferlay J, Lortet-Tieulent J, Jemal A. Global cancer statistics, 2012. CA: a cancer journal for clinicians. 2015;65(2):87-108.
2. Mortality G. Causes of Death C. Causes of Death C. Global, regional, and national age-sex specific all-cause and cause-specific mortality for 240 causes of death, 1990–2013: a systematic analysis for the global burden of disease study 2013. Lancet. 2015;385(9963):117-71.
3. Masters GA, Krilov L, Bailey HH, Brose MS, Burstein H, Diller LR, et al. Clinical cancer advances 2015: annual report on progress against cancer from the American Society of Clinical Oncology. Journal of Clinical Oncology. 2015;33(7):786-809.
4. Zaorsky NG, Churilla T, Egleston B, Fisher S, Ridge J, Horwitz E, et al. Causes of death among cancer patients. Annals of oncology. 2017;28(2):400-7.
5. Gupta GP, Massagué J. Cancer metastasis: building a framework. Cell. 2006;127(4):679-95.
6. Collaborators GRF. Global, regional, and national comparative risk assessment of 79 behavioural, environmental and occupational, and metabolic risks or clusters of risks, 1990–2015: a systematic analysis for the Global Burden of Disease Study 2015. Lancet (London, England). 2016;388(10053):1659.
7. Boroughs LK, DeBerardinis RJ. Metabolic pathways promoting cancer cell survival and growth. Nature cell biology. 2015;17(4):351-9.
8. Pavlova NN, Zhu J, Thompson CB. The hallmarks of cancer metabolism: Still emerging. Cell metabolism. 2022;34(3):355-77.
9. Jang M, Kim SS, Lee J. Cancer cell metabolism: implications for therapeutic targets. Experimental & molecular medicine. 2013;45(10):e45-e.
10. Huang DQ, Singal AG, Kono Y, Tan DJ, El-Serag HB, Loomba R. Changing global epidemiology of liver cancer from 2010 to 2019: NASH is the fastest growing cause of liver cancer. Cell metabolism. 2022;34(7):969-77. e2.
11. Jemal A, Bray F, Center MM, Ferlay J, Ward E, Forman D. Global cancer statistics. CA: a cancer journal for clinicians. 2011;61(2):69-90.

12. Llovet J, Kelley R, Villanueva A, Singal A, Pikarsky E, Roayaie S, et al. Hepatocellular carcinoma Nat Rev Dis Primers. 7: 6. Article10. 2021;1038.
13. Llovet JM, Montal R, Sia D, Finn RS. Molecular therapies and precision medicine for hepatocellular carcinoma. Nature reviews Clinical oncology. 2018;15(10):599-616.
14. Anstee QM, Reeves HL, Kotsiliti E, Govaere O, Heikenwalder M. From NASH to HCC: current concepts and future challenges. Nature reviews Gastroenterology & hepatology. 2019;16(7):411-28.
15. Sherlock S. Causes and effects of acute liver damage. Scandinavian Journal of gastroenterology Supplement. 1970;6:187-202.
16. Custer B, Sullivan SD, Hazlet TK, Iloeje U, Veenstra DL, Kowdley KV. Global epidemiology of hepatitis B virus. Journal of clinical gastroenterology. 2004;38(10):S158-S68.
17. Humans IWGotEoCRt. A review of human carcinogens: Part B: Biological agents: World Health Organisation; 2012.
18. Xess A, KUMAR M, MINZ S, Sharma H, Shahi S. Prevalence of hepatitis B and hepatitis C virus coinfection in chronic liver disease. Indian Journal of Pathology and Microbiology. 2001;44(3):253-5.
19. Cho LY, Yang JJ, Ko KP, Park B, Shin A, Lim MK, et al. Coinfection of hepatitis B and C viruses and risk of hepatocellular carcinoma: systematic review and meta-analysis. International journal of cancer. 2011;128(1):176-84.
20. Donato F, Boffetta P, Puoti M. A meta-analysis of epidemiological studies on the combined effect of hepatitis B and C virus infections in causing hepatocellular carcinoma. International journal of cancer. 1998;75(3):347-54.
21. Shi J, Zhu L, Liu S, Xie W. A meta-analysis of case–control studies on the combined effect of hepatitis B and C virus infections in causing hepatocellular carcinoma in China. British journal of cancer. 2005;92(3):607-12.
22. Berger D, Bradley KA. Primary care management of alcohol misuse. Medical Clinics. 2015;99(5):989-1016.
23. Turati F, Galeone C, Rota M, Pelucchi C, Negri E, Bagnardi V, et al. Alcohol and liver cancer: a systematic review and meta-analysis of prospective studies. Annals of oncology. 2014;25(8):1526-35.

24. Wynder EL, Graham EA. Tobacco smoking as a possible etiologic factor in bronchiogenic carcinoma. Bulletin of the World Health Organization. 2005;83(2):146-53.
25. Humans IWGotEoCRt. Smokeless tobacco. Personal Habits and Indoor Combustions: International Agency for Research on Cancer; 2012.
26. General USPHSOotS. How tobacco smoke causes disease: the biology and behavioral basis for smoking-attributable disease: a report of the Surgeon General: US Department of Health and Human Services, Public Health Service, Office of …; 2010.
27. Chen SY, Wang LY, Lunn RM, Tsai WY, Lee PH, Lee CS, et al. Polycyclic aromatic hydrocarbon-DNA adducts in liver tissues of hepatocellular carcinoma patients and controls. International journal of cancer. 2002;99(1):14-21.
28. Lee Y-CA, Cohet C, Yang Y-C, Stayner L, Hashibe M, Straif K. Meta-analysis of epidemiologic studies on cigarette smoking and liver cancer. International journal of epidemiology. 2009;38(6):1497-511.
29. Gandini S, Botteri E, Iodice S, Boniol M, Lowenfels AB, Maisonneuve P, et al. Tobacco smoking and cancer: a meta-analysis. International journal of cancer. 2008;122(1):155-64.
30. Chuang S-C, Lee Y-CA, Wu G-J, Straif K, Hashibe M. Alcohol consumption and liver cancer risk: a meta-analysis. Cancer Causes & Control. 2015;26:1205-31.
31. Argyo C, Weiss V, Bräuchle C, Bein T. Multifunctional mesoporous silica nanoparticles as a universal platform for drug delivery. Chem Mater. 2014;26(1):435-51.
32. Daniels-Race T. Nanodevices: fabrication, prospects for low dimensional devices and applications. Nanolithography: Elsevier; 2014. p. 399-423.
33. Sully RE, Garelick H, Loizidou EZ, Podoleanu AG, Gubala V. Nanoparticle-infused-biodegradable-microneedles as drug-delivery systems: Preparation and characterisation. Materials Advances. 2021;2(16):5432-42.
34. Boraschi D. How innate and adaptive immunity work. Nanoparticles and the Immune System: Elsevier; 2014. p. 1-7.
35. Siegel RW. Synthesis and properties of nanophase materials. Materials Science and Engineering: A. 1993;168(2):189-97.

36. Gelperina S, Kisich K, Iseman MD, Heifets L. The potential advantages of nanoparticle drug delivery systems in chemotherapy of tuberculosis. American journal of respiratory and critical care medicine. 2005;172(12):1487-90.

37. Slowing II, Vivero-Escoto JL, Wu C-W, Lin VS-Y. Mesoporous silica nanoparticles as controlled release drug delivery and gene transfection carriers. Advanced drug delivery reviews. 2008;60(11):1278-88.

38. Vivero-Escoto JL, Slowing II, Trewyn BG, Lin VSY. Mesoporous silica nanoparticles for intracellular controlled drug delivery. small. 2010;6(18):1952-67.

39. Chung T-H, Wu S-H, Yao M, Lu C-W, Lin Y-S, Hung Y, et al. The effect of surface charge on the uptake and biological function of mesoporous silica nanoparticles in 3T3-L1 cells and human mesenchymal stem cells. Biomaterials. 2007;28(19):2959-66.

40. Lu J, Liong M, Li Z, Zink JI, Tamanoi F. Biocompatibility, biodistribution, and drug-delivery efficiency of mesoporous silica nanoparticles for cancer therapy in animals. small. 2010;6(16):1794-805.

41. Horn D, Rieger J. Organic nanoparticles in the aqueous phase—theory, experiment, and use. Angew Chem Int Ed. 2001;40(23):4330-61.

42. Kumar R, Lal S. Synthesis of organic nanoparticles and their applications in drug delivery and food nanotechnology: a review. J Nanomater Mol Nanotechnol 3: 4. of. 2014;11:2.

43. Huang H-C, Barua S, Sharma G, Dey SK, Rege K. Inorganic nanoparticles for cancer imaging and therapy. J Controlled Release. 2011;155(3):344-57.

44. Na HB, Song IC, Hyeon T. Inorganic nanoparticles for MRI contrast agents. Adv Mater. 2009;21(21):2133-48.

45. Zhang X, Cresswell M. Silica-based amorphous drug delivery systems. Inorganic Controlled Release Technology; Zhang, X, Cresswell, M, Eds. 2016:93-137.

46. Kresge aC, Leonowicz ME, Roth WJ, Vartuli J, Beck J. Ordered mesoporous molecular sieves synthesized by a liquid-crystal template mechanism. nature. 1992;359(6397):710-2.

47. Chiola V, Ritsko JE, Vanderpool CD. Process for producing low-bulk density silica. Google Patents; 1971.

48. Zhao D, Feng J, Huo Q, Melosh N, Fredrickson GH, Chmelka BF, et al. Triblock copolymer syntheses of mesoporous silica with periodic 50 to 300 angstrom pores. science. 1998;279(5350):548-52.

49. Zhao D, Huo Q, Feng J, Chmelka BF, Stucky GD. Nonionic triblock and star diblock copolymer and oligomeric surfactant syntheses of highly ordered, hydrothermally stable, mesoporous silica structures. Journal of the American Chemical Society. 1998;120(24):6024-36.

50. Cao L, Man T, Kruk M. Synthesis of ultra-large-pore SBA-15 silica with two-dimensional hexagonal structure using triisopropylbenzene as micelle expander. Chem Mater. 2009;21(6):1144-53.

51. Zhang H, Sun J, Ma D, Bao X, Klein-Hoffmann A, Weinberg G, et al. Unusual mesoporous SBA-15 with parallel channels running along the short axis. Journal of the American Chemical Society. 2004;126(24):7440-1.

52. Thielemann JP, Girgsdies F, Schlögl R, Hess C. Pore structure and surface area of silica SBA-15: influence of washing and scale-up. Beilstein journal of nanotechnology. 2011;2(1):110-8.

53. Faraji M, Yamini Y, Rezaee M. Magnetic nanoparticles: synthesis, stabilization, functionalization, characterization, and applications. Journal of the Iranian Chemical Society. 2010;7:1-37.

54. Woo K, Hong J, Choi S, Lee H-W, Ahn J-P, Kim CS, et al. Easy synthesis and magnetic properties of iron oxide nanoparticles. Chem Mater. 2004;16(14):2814-8.

55. Gupta AK, Gupta M. Synthesis and surface engineering of iron oxide nanoparticles for biomedical applications. biomaterials. 2005;26(18):3995-4021.

56. Schwertmann U, Cornell R. Iron oxides in the laboratory. VCH, Weinheim Germany; 1991.

57. Lin MM, Kim DK, El Haj AJ, Dobson J. Development of superparamagnetic iron oxide nanoparticles (SPIONS) for translation to clinical applications. IEEE transactions on nanobioscience. 2008;7(4):298-305.

58. Mahmoudi M, Sant S, Wang B, Laurent S, Sen T. Superparamagnetic iron oxide nanoparticles (SPIONs): development, surface modification and applications in chemotherapy. Advanced drug delivery reviews. 2011;63(1-2):24-46.

59. Chen H, Yeh J, Wang L, Khurshid H, Peng N, Wang AY, et al. Preparation and control of the formation of single core and clustered nanoparticles for biomedical applications using a versatile amphiphilic diblock copolymer. Nano Research. 2010;3:852-62.

60. Rozhkova EA. Nanoscale materials for tackling brain cancer: Recent progress and outlook. Adv Mater. 2011;23(24):H136-H50.

61. Yin Y, Alivisatos AP. Colloidal nanocrystal synthesis and the organic–inorganic interface. Nature. 2005;437(7059):664-70.

62. Wáng Y-XJ, Choi Y, Chen Z, Laurent S, Gibbs SL. Molecular imaging: from bench to clinic. BioMed Research International. 2014;2014:357258.

63. Lu AH, Salabas EeL, Schüth F. Magnetic nanoparticles: synthesis, protection, functionalization, and application. Angew Chem Int Ed. 2007;46(8):1222-44.

64. Sonmez M, Georgescu M, Alexandrescu L, Gurau D, Ficai A, Ficai D, et al. Synthesis and applications of Fe3O4/SiO2 core-shell materials. Current pharmaceutical design. 2015;21(37):5324-35.

65. Stöber W, Fink A, Bohn E. Controlled growth of monodisperse silica spheres in the micron size range. J Colloid Interface Sci. 1968;26(1):62-9.

66. Helmi Rashid Farimani M, Shahtahmassebi N, Rezaee Roknabadi M, Ghows N. Synthesis and study of structural and magnetic properties of superparamagnetic Fe3O4@ SiO2 core/shell nanocomposite for biomedical applications. Nanomedicine Journal. 2014;1(2):71-8.

67. Narita A, Naka K, Chujo Y. Facile control of silica shell layer thickness on hydrophilic iron oxide nanoparticles via reverse micelle method. Colloids and Surfaces A: Physicochemical and Engineering Aspects. 2009;336(1-3):46-56.

68. Ding H, Zhang Y, Wang S, Xu J, Xu S, Li G. Fe3O4@ SiO2 core/shell nanoparticles: the silica coating regulations with a single core for different core sizes and shell thicknesses. Chem Mater. 2012;24(23):4572-80.

69. Lu C-W, Hung Y, Hsiao J-K, Yao M, Chung T-H, Lin Y-S, et al. Bifunctional magnetic silica nanoparticles for highly efficient human stem cell labeling. Nano Lett. 2007;7(1):149-54.

70. Philipse AP, Van Bruggen MP, Pathmamanoharan C. Magnetic silica dispersions: preparation and stability of surface-modified silica particles with a magnetic core. Langmuir. 1994;10(1):92-9.
71. Van Ewijk G, Vroege G, Philipse A. Convenient preparation methods for magnetic colloids. J Magn Magn Mater. 1999;201(1-3):31-3.
72. Deng Y-H, Wang C-C, Hu J-H, Yang W-L, Fu S-K. Investigation of formation of silica-coated magnetite nanoparticles via sol–gel approach. Colloids and Surfaces A: Physicochemical and Engineering Aspects. 2005;262(1-3):87-93.
73. Barnakov YA, Yu MH, Rosenzweig Z. Manipulation of the magnetic properties of magnetite− silica nanocomposite materials by controlled stober synthesis. Langmuir. 2005;21(16):7524-7.
74. Sun Y, Duan L, Guo Z, DuanMu Y, Ma M, Xu L, et al. An improved way to prepare superparamagnetic magnetite-silica core-shell nanoparticles for possible biological application. J Magn Magn Mater. 2005;285(1-2):65-70.
75. Gao M, Li W, Dong J, Zhang Z, Yang B. Synthesis and characterization of superparamagnetic Fe3O4@ SiO2 core-shell composite nanoparticles. World Journal of Condensed Matter Physics. 2011;1(2):49-54.
76. Kulkarni SA, Sawadh P, Palei PK. Synthesis and characterization of superparamagnetic Fe 3 O 4@ SiO 2 nanoparticles. J Korean Chem Soc. 2014;58(1):100-4.
77. Gupta AK, Wells S. Surface-modified superparamagnetic nanoparticles for drug delivery: preparation, characterization, and cytotoxicity studies. IEEE transactions on nanobioscience. 2004;3(1):66-73.
78. Santra S, Tapec R, Theodoropoulou N, Dobson J, Hebard A, Tan W. Synthesis and characterization of silica-coated iron oxide nanoparticles in microemulsion: the effect of nonionic surfactants. Langmuir. 2001;17(10):2900-6.
79. Wu S-H, Mou C-Y, Lin H-P. Synthesis of mesoporous silica nanoparticles. Chem Soc Rev. 2013;42(9):3862-75.
80. Slowing II, Trewyn BG, Giri S, Lin VY. Mesoporous silica nanoparticles for drug delivery and biosensing applications. Adv Funct Mater. 2007;17(8):1225-36.
81. Tang F, Li L, Chen D. Mesoporous silica nanoparticles: synthesis, biocompatibility and drug delivery. Adv Mater. 2012;24(12):1504-34.

82. Wu P, Zhu J, Xu Z. Template-assisted synthesis of mesoporous magnetic nanocomposite particles. Adv Funct Mater. 2004;14(4):345-51.

83. Zhao W, Gu J, Zhang L, Chen H, Shi J. Fabrication of uniform magnetic nanocomposite spheres with a magnetic core/mesoporous silica shell structure. Journal of the American Chemical Society. 2005;127(25):8916-7.

84. Deng Y, Qi D, Deng C, Zhang X, Zhao D. Superparamagnetic high-magnetization microspheres with an Fe3O4@ SiO2 core and perpendicularly aligned mesoporous SiO2 shell for removal of microcystins. Journal of the American Chemical Society. 2008;130(1):28-9.

85. El-Toni AM, Ibrahim MA, Labis JP, Khan A, Alhoshan M. Optimization of synthesis parameters for mesoporous shell formation on magnetic nanocores and their application as nanocarriers for docetaxel cancer drug. International journal of molecular sciences. 2013;14(6):11496-509.

86. Xue S, Wang Y, Wang M, Zhang L, Du X, Gu H, et al. Iodinated oil-loaded, fluorescent mesoporous silica-coated iron oxide nanoparticles for magnetic resonance imaging/computed tomography/fluorescence trimodal imaging. International Journal of Nanomedicine. 2014:2527-38.

87. Rizvi SA, Saleh AM. Applications of nanoparticle systems in drug delivery technology. Saudi pharmaceutical journal. 2018;26(1):64-70.

88. Shi Y, Lammers T. Combining nanomedicine and immunotherapy. Acc Chem Res. 2019;52(6):1543-54.

89. Zwicke GL, Ali Mansoori G, Jeffery CJ. Utilizing the folate receptor for active targeting of cancer nanotherapeutics. Nano reviews. 2012;3(1):18496.

90. Cooper GM, Hausman R. A molecular approach. The Cell 2nd ed Sunderland, MA: Sinauer Associates. 2000:1394-403.

91. Xu T, Ding W, Ji X, Ao X, Liu Y, Yu W, et al. Molecular mechanisms of ferroptosis and its role in cancer therapy. Journal of cellular and molecular medicine. 2019;23(8):4900-12.

92. Liang C, Zhang X, Yang M, Dong X. Recent progress in ferroptosis inducers for cancer therapy. Advanced materials. 2019;31(51):1904197.

93. Nie Q, Hu Y, Yu X, Li X, Fang X. Induction and application of ferroptosis in cancer therapy. Cancer cell international. 2022;22(1):12.

94. Kumari A, Yadav SK, Yadav SC. Biodegradable polymeric nanoparticles based drug delivery systems. Colloids and surfaces B: biointerfaces. 2010;75(1):1-18.
95. Hans ML, Lowman AM. Biodegradable nanoparticles for drug delivery and targeting. Curr Opin Solid State Mater Sci. 2002;6(4):319-27.
96. Liu Z, Jiao Y, Wang Y, Zhou C, Zhang Z. Polysaccharides-based nanoparticles as drug delivery systems. Advanced drug delivery reviews. 2008;60(15):1650-62.
97. Chen J-F, Ding H-M, Wang J-X, Shao L. Preparation and characterization of porous hollow silica nanoparticles for drug delivery application. Biomaterials. 2004;25(4):723-7.
98. Lu J, Liong M, Zink JI, Tamanoi F. Mesoporous silica nanoparticles as a delivery system for hydrophobic anticancer drugs. small. 2007;3(8):1341-6.
99. Kalluri R, Weinberg RA. The basics of epithelial-mesenchymal transition. The Journal of clinical investigation. 2009;119(6):1420-8.
100. Lee JM, Dedhar S, Kalluri R, Thompson EW. The epithelial–mesenchymal transition: new insights in signaling, development, and disease. The Journal of cell biology. 2006;172(7):973-81.
101. Hanahan D, Weinberg RA. Hallmarks of cancer: the next generation. cell. 2011;144(5):646-74.
102. Ibrahim MMA. Assessment of Epithelial-mesenchymal Transition and Tumor Stroma Ratio via Vimentin Expression in Salivary Adenoid Cystic Carcinoma. Mansoura Journal of Dentistry. 2023;11(3):1.
103. Jou J, Diehl AM. Epithelial-mesenchymal transitions and hepatocarcinogenesis. The Journal of clinical investigation. 2010;120(4):1031-4.
104. Xu Q, Liu X, Liu Z, Zhou Z, Wang Y, Tu J, et al. MicroRNA-1296 inhibits metastasis and epithelial-mesenchymal transition of hepatocellular carcinoma by targeting SRPK1-mediated PI3K/AKT pathway. Molecular cancer. 2017;16:1-15.
105. Ren D, Yang Q, Dai Y, Guo W, Du H, Song L, et al. Oncogenic miR-210-3p promotes prostate cancer cell EMT and bone metastasis via NF-κB signaling pathway. Molecular cancer. 2017;16:1-16.
106. Tang F-Y, Pai M-H, Chiang E-PI. Consumption of high-fat diet induces tumor progression and epithelial–mesenchymal transition of colorectal cancer in a mouse xenograft model. The Journal of nutritional biochemistry. 2012;23(10):1302-13.

107. Zhang P, Li K, Shen Y, Gao P, Dong Z, Cai J, et al. Galectin-1 induces hepatocellular carcinoma EMT and sorafenib resistance by activating FAK/PI3K/AKT signaling. Cell death & disease. 2016;7(4):e2201-e.

108. Bolós V, Peinado H, Pérez-Moreno MA, Fraga MF, Esteller M, Cano A. The transcription factor Slug represses E-cadherin expression and induces epithelial to mesenchymal transitions: a comparison with Snail and E47 repressors. J Cell Sci. 2003;116(3):499-511.

109. Qiao M, Sheng S, Pardee AB. Metastasis and AKT activation. Cell cycle. 2008;7(19):2991-6.

110. Wang Y, Shi J, Chai K, Ying X, P Zhou B. The role of snail in EMT and tumorigenesis. Current cancer drug targets. 2013;13(9):963-72.

111. Yoo YA, Kang MH, Lee HJ, Kim B-h, Park JK, Kim HK, et al. Sonic hedgehog pathway promotes metastasis and lymphangiogenesis via activation of Akt, EMT, and MMP-9 pathway in gastric cancer. Cancer research. 2011;71(22):7061-70.

112. Zuo JH, Zhu W, Li MY, Li XH, Yi H, Zeng GQ, et al. Activation of EGFR promotes squamous carcinoma SCC10A cell migration and invasion via inducing EMT-like phenotype change and MMP-9-mediated degradation of E-cadherin. J Cell Biochem. 2011;112(9):2508-17.

113. Siegel RL, Miller KD, Wagle NS, Jemal A. Cancer statistics, 2023. CA: a cancer journal for clinicians. 2023;73(1):17-48.

114. Balogh J, Victor III D, Asham EH, Burroughs SG, Boktour M, Saharia A, et al. Hepatocellular carcinoma: a review. Journal of hepatocellular carcinoma. 2016:41-53.

115. Bruix J, Sherman M. Management of hepatocellular carcinoma. Hepatology. 2005;42(5):1208-36.

116. Dang Y, Guan J. Nanoparticle-based drug delivery systems for cancer therapy. Smart materials in medicine. 2020;1:10-9.

117. Chandrakala V, Aruna V, Angajala G. Review on metal nanoparticles as nanocarriers: Current challenges and perspectives in drug delivery systems. Emergent Materials. 2022;5(6):1593-615.

118. Huang Y, Li P, Zhao R, Zhao L, Liu J, Peng S, et al. Silica nanoparticles: Biomedical applications and toxicity. Biomedicine & Pharmacotherapy. 2022;151:113053.
119. Manzano M, Vallet-Regí M. Mesoporous silica nanoparticles for drug delivery. Adv Funct Mater. 2020;30(2):1902634.
120. Albayati TM, Alardhi SM, Khalbas AH, Humdi ZJ, Ali NS, Salih IK, et al. Comprehensive review of mesoporous silica nanoparticles: drug loading, release, and applications as hemostatic agents. ChemistrySelect. 2024;9(23):e202400450.
121. Tufani A, Qureshi A, Niazi JH. Iron oxide nanoparticles based magnetic luminescent quantum dots (MQDs) synthesis and biomedical/biological applications: A review. Materials Science and Engineering: C. 2021;118:111545.
122. Pal N, Lee J-H, Cho E-B. Recent trends in morphology-controlled synthesis and application of mesoporous silica nanoparticles. Nanomaterials. 2020;10(11):2122.
123. Kankala RK, Han YH, Na J, Lee CH, Sun Z, Wang SB, et al. Nanoarchitectured structure and surface biofunctionality of mesoporous silica nanoparticles. Adv Mater. 2020;32(23):1907035.
124. Pellicer-Castell E, Belenguer-Sapiña C, El Haskouri J, Amorós P, Herrero-Martínez JM, Mauri-Aucejo AR. Iron-Doped Bimodal Mesoporous Silica Nanomaterials as Sorbents for Solid-Phase Extraction of Perfluoroalkyl Substances in Environmental Water Samples. Nanomaterials. 2022;12(9):1441.
125. Mdlovu NV, Lin K-S, Mavuso FA, Weng M-T. Preparation, characterization, and in-vitro studies of doxorubicin-encapsulated silica coated iron oxide nanocomposites on liver cancer cells. Journal of the Taiwan Institute of Chemical Engineers. 2020;117:190-7.
126. Coelho JV, Guedes MS, Prado RG, Tronto J, Ardisson JD, Pereira MC, et al. Effect of iron precursor on the Fenton-like activity of Fe2O3/mesoporous silica catalysts prepared under mild conditions. Applied Catalysis B: Environmental. 2014;144:792-9.
127. Candela-Noguera V, Amorós P, Aznar E, Marcos MD, Martínez-Máñez R. Systematic study of the implications of calcination and solvent extraction of the surfactant in MCM-41-type mesoporous silica nanoparticles. Microporous Mesoporous Mater. 2024;373:113119.

128. Sarikhani AR, Abedi M, Abolmaali SS, Borandeh S, Tamaddon AM. Magnetic graphene oxide nanosheets with amidoamine dendronized crosslinks for dual pH and redox-sensitive doxorubicin delivery. BMC chemistry. 2024;18(1):189.
129. Kumar CS, Raja M, Sundar DS, Antoniraj MG, Ruckmani K. Hyaluronic acid co-functionalized gold nanoparticle complex for the targeted delivery of metformin in the treatment of liver cancer (HepG2 cells). Carbohydr Polym. 2015;128:63-74.
130. Lin T-T, Gao D-Y, Liu Y-C, Sung Y-C, Wan D, Liu J-Y, et al. Development and characterization of sorafenib-loaded PLGA nanoparticles for the systemic treatment of liver fibrosis. J Controlled Release. 2016;221:62-70.
131. Ruman U, Buskaran K, Pastorin G, Masarudin MJ, Fakurazi S, Hussein MZ. Synthesis and characterization of chitosan-based nanodelivery systems to enhance the anticancer effect of sorafenib drug in hepatocellular carcinoma and colorectal adenocarcinoma cells. Nanomaterials. 2021;11(2):497.
132. Chen K, Chang C, Liu Z, Zhou Y, Xu Q, Li C, et al. Hyaluronic acid targeted and pH-responsive nanocarriers based on hollow mesoporous silica nanoparticles for chemo-photodynamic combination therapy. Colloids and Surfaces B: Biointerfaces. 2020;194:111166.
133. Amjad Q, Shakoori AR. Recombinant Slit2 Requires Heparin Sulphate to Inhibit TGF-ß Induced Tumor Proliferation in Lung Cancer and Glioblastoma. Pakistan Journal of Zoology. 2024;56(5).
134. Amjad Q, Stein GS, van Wijnen AJ, Shakoori AR. Cancer Cell-Type-Dependent Modifications of Metastatic Parameters by SLIT2-ROBO1 and RHOA cAMP Signaling in Response to TGFβ1 and FGF2. Critical Reviews™ in Eukaryotic Gene Expression. 2024;34(7).
135. Mdlovu NV, Lin K-S, Weng M-T, Hsieh C-C, Lin Y-S, Espinoza MJC. In vitro intracellular studies of pH and thermo-triggered doxorubicin conjugated magnetic SBA-15 mesoporous nanocarriers for anticancer activity against hepatocellular carcinoma. Journal of Industrial and Engineering Chemistry. 2021;102:1-16.
136. Barraud L, Merle P, Soma E, Lefrançois L, Guerret S, Chevallier M, et al. Increase of doxorubicin sensitivity by doxorubicin-loading into nanoparticles for

hepatocellular carcinoma cells in vitro and in vivo. Journal of hepatology. 2005;42(5):736-43.

137. Varlamova EG, Goltyaev MV, Simakin AV, Gudkov SV, Turovsky EA. Comparative analysis of the cytotoxic effect of a complex of selenium nanoparticles doped with sorafenib,“naked” selenium nanoparticles, and sorafenib on human hepatocyte carcinoma HepG2 cells. International Journal of Molecular Sciences. 2022;23(12):6641.

138. Madhavi, Kumar M, Ansari JR, Kumar V, Nagar S, Sharma A. Fe3O4 coated SiO2 magnetic nanoparticles for enhanced antibacterial activity and electrochemical sensing. Metals. 2022;12(12):2145.

139. Yaseen M, Khan A, Humayun M, Farooq S, Shah N, Bibi S, et al. Facile synthesis of Fe3O4− SiO2 nanocomposites for wastewater treatment. Macromolecular Materials and Engineering. 2023;308(7):2200695.

140. García-Vidal U, Jiménez-Pérez J, Correa-Pacheco Z, López-Gamboa G, Gutiérrez-Fuentes R, Luna-Sánchez J. Thermal study of ferromagnetic nanoparticles coated with silicon oxide. Int J Thermophys. 2023;44(2):18.

141. Arshad M, Abbas M, Ehtisham-ul-Haque S, Farrukh MA, Ali A, Rizvi H, et al. Synthesis and characterization of SiO2 doped Fe2O3 nanoparticles: Photocatalytic and antimicrobial activity evaluation. J Mol Struct. 2019;1180:244-50.

142. Tabasi H, Mosavian MTH, Darroudi M, Khazaei M, Hashemzadeh A, Sabouri Z. Synthesis and characterization of amine-functionalized Fe3O4/Mesoporous Silica Nanoparticles (MSNs) as potential nanocarriers in drug delivery systems. J Porous Mater. 2022;29(6):1817-28.

143. Wang J, Zheng S, Shao Y, Liu J, Xu Z, Zhu D. Amino-functionalized Fe3O4@ SiO2 core–shell magnetic nanomaterial as a novel adsorbent for aqueous heavy metals removal. J Colloid Interface Sci. 2010;349(1):293-9.

144. Han JS, An GS. Preparation of dual-layered core–shell Fe3O4@ SiO2 nanoparticles and their properties of plasmid DNA purification. Nanomaterials. 2021;11(12):3422.

145. Gemeay AH, Keshta BE, El-Sharkawy RG, Zaki AB. Chemical insight into the adsorption of reactive wool dyes onto amine-functionalized magnetite/silica core-

shell from industrial wastewaters. Environmental Science and Pollution Research. 2020;27:32341-58.

146. Tang H, Chen D, Li C, Zheng C, Wu X, Zhang Y, et al. Dual GSH-exhausting sorafenib loaded manganese-silica nanodrugs for inducing the ferroptosis of hepatocellular carcinoma cells. Int J Pharm. 2019;572:118782.